AD-A243 384

||||||||||||||||||||||||||||

	2. REPORT DATE	3. REPORT TYPE AND DATES COVERED
	August 1991	~~THESIS~~/DISSERTATION

4. TITLE AND SUBTITLE	5. FUNDING NUMBERS
The Analysis of a Stabilized 1.5 Mach-Zehnder Interferometric Sensor with Enhanced Sensitivity and Common-Mode Compensation	

6. AUTHOR(S)

Booker Howell Tyrone, Jr.,Captain

7. PERFORMING ORGANIZATION NAME(S) AND ADDRESS(ES)	8. PERFORMING ORGANIZATION REPORT NUMBER
AFIT Student Attending: University of Texas	AFIT/CI/CIA- 91-014D

9. SPONSORING/MONITORING AGENCY NAME(S) AND ADDRESS(ES)	10. SPONSORING/MONITORING AGENCY REPORT NUMBER
AFIT/CI Wright-Patterson AFB OH 45433-6583	

11. SUPPLEMENTARY NOTES

12a. DISTRIBUTION/AVAILABILITY STATEMENT	12b. DISTRIBUTION CODE
Approved for Public Release IAW 190-1 Distributed Unlimited ERNEST A. HAYGOOD, Captain, USAF Executive Officer	

13. ABSTRACT *(Maximum 200 words)*

14. SUBJECT TERMS		15. NUMBER OF PAGES
		95
		16. PRICE CODE

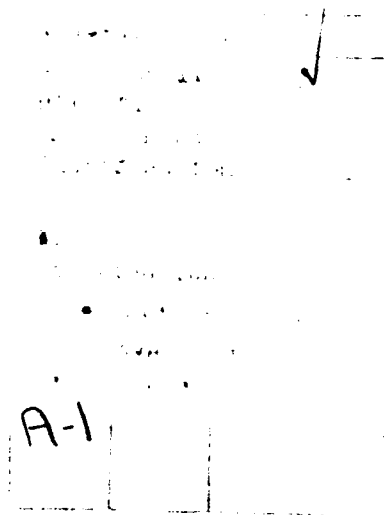| 17. SECURITY CLASSIFICATION OF REPORT	18. SECURITY CLASSIFICATION OF THIS PAGE	19. SECURITY CLASSIFICATION OF ABSTRACT	20. LIMITATION OF ABSTRACT

THE ANALYSIS OF A STABILIZED 1.5 MACH-ZEHNDER INTERFEROMETRIC SENSOR WITH ENHANCED SENSITIVITY AND COMMON-MODE COMPENSATION

A-1

APPROVED BY
DISSERTATION COMMITTEE:

91 1213 138

Dedication

I dedicate this work to my father, Booker H. Tyrone, Sr.,

my mother, Hattie M. Tyrone,

and my aunts, Ankalena E. Chambers and S. Ruthester Parker.

It was their encouragement that kindled the desire within me to succeed.

THE ANALYSIS OF A STABILIZED 1.5 MACH-ZEHNDER INTERFEROMETRIC SENSOR WITH ENHANCED SENSITIVITY AND COMMON-MODE COMPENSATION

by

BOOKER HOWELL TYRONE, JR., B.S.E.E., M.S.E.

DISSERTATION

Presented to the Faculty of the Graduate School of

The University of Texas at Austin

in Partial Fulfillment

of the Requirements

for the Degree of

DOCTOR OF PHILOSOPHY

THE UNIVERSITY OF TEXAS AT AUSTIN

August 1991

Acknowledgements

I wish to express my sincerest gratitude to Dr. A. Bruce Buckman for his invaluable guidance and support throughout this research. His patience and positive approach made my studies under his tutelage an enlightening and enjoyable experience. I also want to thank the members of my committee: Dr. Michael F. Becker, Dr. Ilene J. Busch-Vishniac, Dr. Joe C. Campbell, and Dr. Elmer L. Hixson. Their interest in my research and the knowledge which they imparted to me have immensely benefitted my research efforts.

I want to thank my colleagues, Franklin Y. Cheung, Lisa Guilianelli, Chellappan Narayanan, Aaron Seltzer, and John D. Wheelis, for their helpful suggestions and comments. Often they asked questions which focussed my efforts towards the correct solutions. Without the use of the simulation programs written by Aaron Seltzer and Dr. Buckman, I would have expended many hours determining the expected performance of this sensor. Their programs allowed me to illustrate with figures rather than equations the simulated outputs derived from this sensor. I must thank Mr. Wayne Wehrer and the technicians involved with building the controller prototype. Their technical experience saved me numerous months of work and furthered my efforts toward timely completion. Also, I owe a debt of gratitude to Mr. Norman Williams and Mr. John Spurgeon for their technical advice regarding methods to overcome noise problems and efficiently design circuits. To all those who contributed in some manner to the successful completion of this project but are not individually named, I offer a most genuine thank you.

My sincere appreciation is extended to the leadership of the United States Air Force Academy (USAFA) for giving me this opportunity to complete my Ph.D. A

THE ANALYSIS OF A STABILIZED 1.5 MACH-ZEHNDER INTERFEROMETRIC SENSOR WITH ENHANCED SENSITIVITY AND COMMON-MODE COMPENSATION

Publication No._____

Booker Howell Tyrone, Jr., Ph.D.

The University of Texas at Austin, 1991

Supervising Professor: A. Bruce Buckman

The design and construction of an active stabilization controller and its interface to an interferometric fiber optic sensor--the enhanced sensitivity, common-mode compensated 1.5 Mach-Zehnder [1] is reported in this dissertation. The feasibility of employing this active stabilization circuit to maintain the operation of an enhanced sensitivity, common-mode compensated 1.5 Mach-Zehnder interferometer over the narrow operating range required for common-mode compensation and high sensitivity was demonstrated. Thus, a suitable means to minimize, even eliminate, the effects of environmental disturbances (common-mode and random) and to achieve maximum sensitivity and linearity in the presence of differential phase modulation was proven. This research shows that the incorporation of a controller into the fiber optic sensor can improve the performance of the sensor with electro-optic feedback over two orders of

magnitude (100 times) more than without electro-optic feedback. More importantly, the fiber optic sensor exhibited nearly a full order of magnitude (10 times) improvement in sensitivity beyond the state-of-the-art performance reported to date [42] for the conventional Mach-Zehnder optical circuit.

Table of Contents

List of Tables

List of Figures

Chapter 1
Introduction

The objective of this dissertation is to extensively describe how the implementation of an electronic/optical system to actively control the phase biases of an enhanced sensitivity, common-mode compensated, 1.5 Mach-Zehnder [1] interferometric sensor maintains the sensor's operation over the narrow range required for common-mode compensation (suppression of noises common to all paths within the optical circuit) and high sensitivity. The sensor is, thereby, able to measure minimum detectable phase shifts exceeding the current state-of-the-art performance of conventional Mach-Zehnder interferometers by nearly a full order of magnitude. Previous work employing the 1.5 Mach-Zehnder by Buckman, Park, and Pritchett [2] demonstrated, in a free-running mode only, the existence of high sensitivity regions with common-mode compensation (CMC). The stability of the sensor in the earlier experiments made verification of the minimum detectable phase shift reliably unquantifiable. However, the sensitivity of the sensor was estimated from calculations of the maximum slope achievable for the sensor's output. In an effort to quantify the minimum detectable phase shift measurable by the sensor, a method to stabilize the sensor in the presence of common-mode and random environmental noises was sought. The investigation of stabilization efforts led to the construction of a phase tracking controller which could be directly incorporated into the sensor system. The active stabilization of the 1.5 Mach-Zehnder interferometer (MZI) resulted in a minimum detectable phase shift of 0.09 μ radian/$\sqrt{\text{Hz}}$ being measured.

In this dissertation, the operation of the controller and the fiber optic sensor (FOS) is detailed, and a quantitative analysis of the sensor's performance is given. Chapter 1 reveals the role of fiber optics in sensor applications and identifies the sensor classifications. Chapter 2 describes, in general, interferometric sensor operation and, more specifically, the operation of the 1.0 and 1.5 Mach-Zehnder. Chapters 3 and 4 examine the relationships between the phase biases and the electro-optic feedback gain of the 1.5 Mach-Zehnder used to minimize common-mode noise effects and maximize the sensor's sensitivity. Computer simulations illustrate the effects of common-mode compensation and electro-optic feedback (EOF) on the sensor's transmittance curves. The theory of operation and the details of the construction of the active stabilization controller are explained in Chapter 5. The experimental set-up and results are specified in Chapter 6. Finally, Chapter 7 contains the summary and concluding remarks.

1.1. Role of Fiber Optics in Sensor Technology

In 1977 serious development of fiber optic sensors began with the realization that the sensitivity of fiber optic transducers could be incredible if the quantum shot noise limit could be reached. Since then progress has been rapid. The growth of participants in national and international conferences devoted to these sensors indicate the emergence of the fiber optic sensor technology as an accurate, sensitive, and robust means for measuring physical variables in industrial, avionic, medical, and military applications. Numerous schemes have been envisioned for measuring liquid levels, displacement, strain, torque, fluid flow, acceleration, rotation rate, etc...[3]; fiber optic sensor applications are diverse. Today, they encompass medical diagnostics, guidance

and navigation, robotics, industrial control, power generation, environmental monitoring, and sonar [4]. The world commercial market for fiber optic sensors is projected to reach $814 million annually by 1998 [5]. The potential for this technology is widely acknowledged, yet the long lead times required to adapt new technology to mass production delay its ascension to a more prominent role.

Recent advances in technology accompanied by unrelenting pressures to reduce cost, improve accuracy and reliability, and replace inadequate or unsatisfactory traditional methods in industry have fueled efforts to develop fiber optic sensors. The driving force for fiber optics is its inherent advantages over competing sensor technology. Fiber optic sensors are dielectric devices that demonstrate high sensitivity, immunity from radio-frequency or electromagnetic interference, and geometric versatility [6]. They are safe to operate in areas of high voltage, explosive hazards, corrosion, and extreme temperatures. They can detect physical perturbations in sound, displacement, temperature, pressure, magnetic fields, electric fields, rotation rate, strain, liquid level and flow, and chemical concentration[7]. Their light weight, small size, and lack of moving parts make them a major target for military and aerospace use [8]. Additionally, two attractive features of the optical fibers utilized to manufacture the sensors are its low signal attenuation and high information transfer capacity.

Many specific applications exploit the advantages of fiber optic sensors. For example, the medical diagnostic sensors use the small cross-section of optical fibers to allow physicians to peer inside the body without surgery. Fiber optic thermometers are utilized in cancer treatment where microwave radiation therapy precludes using any conventional electronic sensors. Due to its freedom from radio-frequency and electromagnetic interference, the military employs fiber optics to preserve a high degree

of privacy in electrically noisy environments . The light weight and small size of fiber optic sensors have attracted designers of aircraft and satellites. Similarly, automakers envision centralized control of remote sensors. In the power industry, fiber optic sensors play a minor yet important role of monitoring communications and control functions. Its relative inertness to hazardous or extreme environments has made fiber optics ideal for measurements in jet engines, nuclear reactors, and transformers. Refineries and chemical plants are seeking fiber optic sensors to avoid sparks in an atmosphere contaminated with explosive gases. Barring any unforeseen changes in technology, the role of fiber optics will continue to expand within the sensor industry.

1.2. Types of Fiber Optic Sensors

Fiber optic sensors can be broken down into several major subcategories; however, the two most frequent classifications of fiber optic sensors are intensity (amplitude) and interferometric (phase) sensors. Since the sensor utilized in this analysis is of the interferometric type, the intensity sensor is briefly described here only for completeness. The interferometric sensor is examined in detail in Chapter 2.

The earliest fiber optic sensors implemented were the intensity-modulated type. They employ optical fibers to convey light but use external phenomena such as reflection from a target or attenuation in an absorbing medium for the actual measurement. Physical perturbations modulate the intensity or spectral content of the light propagating in the fiber or through optical elements connected by fibers. The light beam is either detected upon transmission or upon reflection in the interaction region.

Fig. 1 shows the general form of an intensity-modulated sensor and indicates the most often used intensity modulation mechanisms [9].

The principal virtues of intensity sensors are simplicity of design, low cost, reliability, compatibility with today's multimode and single-mode fiber technology, and adequate sensitivity for many applications. These sensors employ relatively simple optics (LED or laser diode light sources), many of which produce no noise in excess of quantum shot noise. These sensors can incorporate time multiplexing techniques without dispatching external electric power to the sensor location.

While intensity sensors are attractive in their inherent simplicity, they are prone to errors due to critical mechanical alignment, variations in losses along fiber paths, fluctuations in the optical source intensity, and long term instability of photodetector sensitivity. Connectors are necessary between source and fiber and detector because most intensity modulation mechanisms require a break in the optical path. These mechanical couplings are another source of losses. Some clever forms of referencing have been developed to allow for coupler and source introduced anomalies; however, this increases the complexity and cost. [10].

To date, the best sensitivities that can be attained with intensity-modulated devices, in terms of minimum detectable displacements of mechanical-motion detectors, lie in the range of 10^{-10} to 10^{-7} meter as compared with the lower limit of 10^{-14} meter achievable with interferometric type sensors [11]. This diminished sensitivity has been adequate in applications where sensitivity is not paramount. Presently, the majority of fiber optic sensors commercially available are intensity sensors for industrial, chemical, and biomedical applications. Increasingly, however, interest is turning to the interferometric sensors as promising applications requiring greater
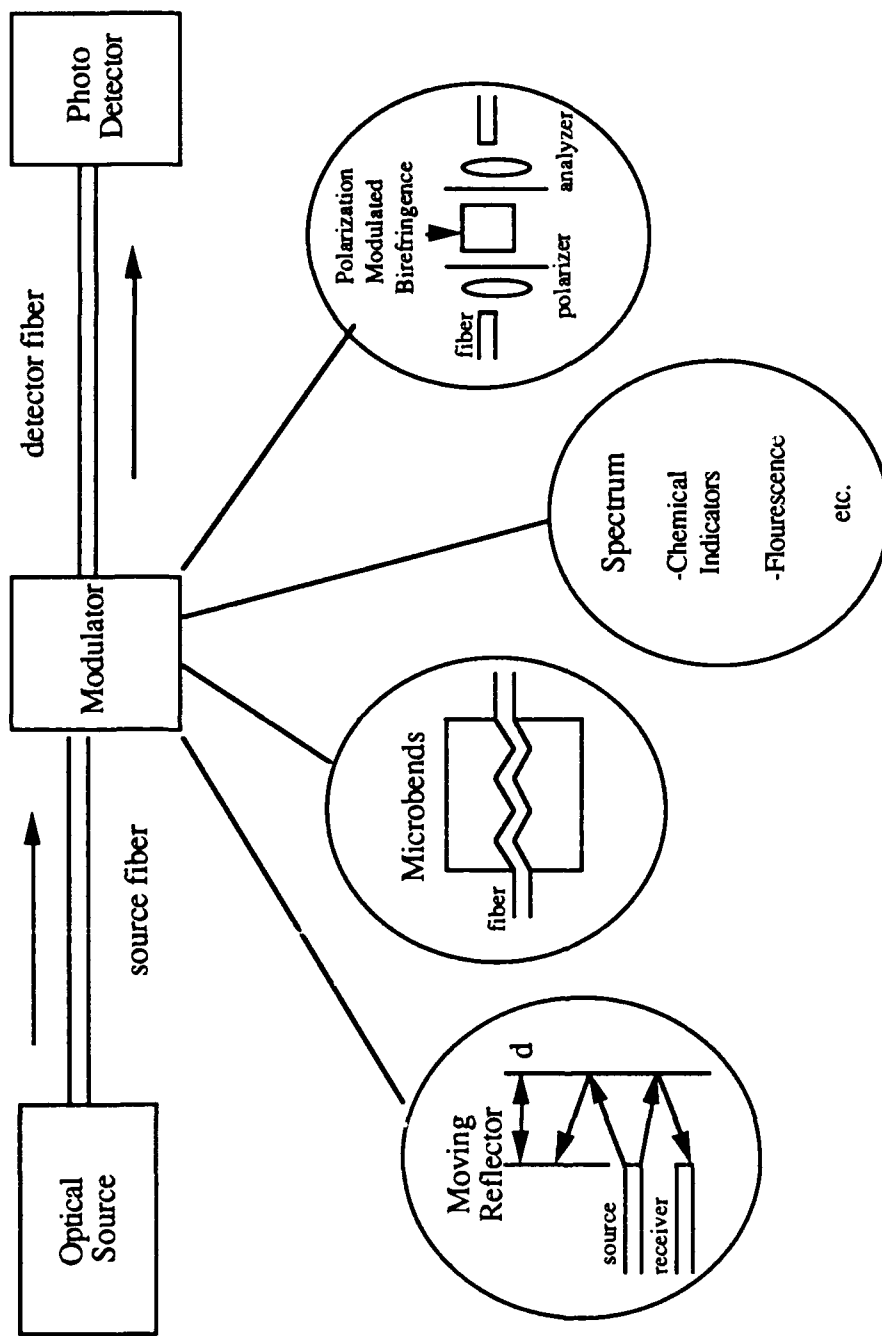
Fig. 1. General Intensity-Modulated Sensor Configuration and Mechanisms[9]

sensitivity and geometric flexibility (than is offered by intensity sensors) are discovered. Interferometric sensors are the subject of the next chapter.

Chapter 2
Interferometric Sensors

In a wide variety of applications, the interferometric fiber optic sensors have demonstrated an enormously greater sensitivity than the intensity sensors and other existing technologies. They derive measurement information directly from the interaction between the light in the fibers and the phenomena of interest (e.g., strain, pressure, temperature, etc.). Phase shifts of the light propagating in the fiber are induced by altering the diameter of the fiber core, the fiber length, and /or the refractive indices of the core and cladding. Because the optical frequency exceeds the response of the photodetectors, optical interferometers are used to convert phase modulation to amplitude modulation by producing an interference pattern. Numerous configurations of fiber optic interferometers are being developed as sensors, and Table 1 identifies the best known of these [12]:

Table 1. Fiber optic interferometric configurations [12]

Differential	Classical Interferometric	Hybrid Systems
1. Polarimetric	Two Beam	1. Laser Doppler
2. Magneto-optical	1. Mach-Zehnder	Velocimetry
	2. Michelson	2. Remote Interferometry
	3. Sagnac	
	4. Fizeau	
	Multiple Beam	
	1. Fabry Perot	
	2. Ring resonator	

9

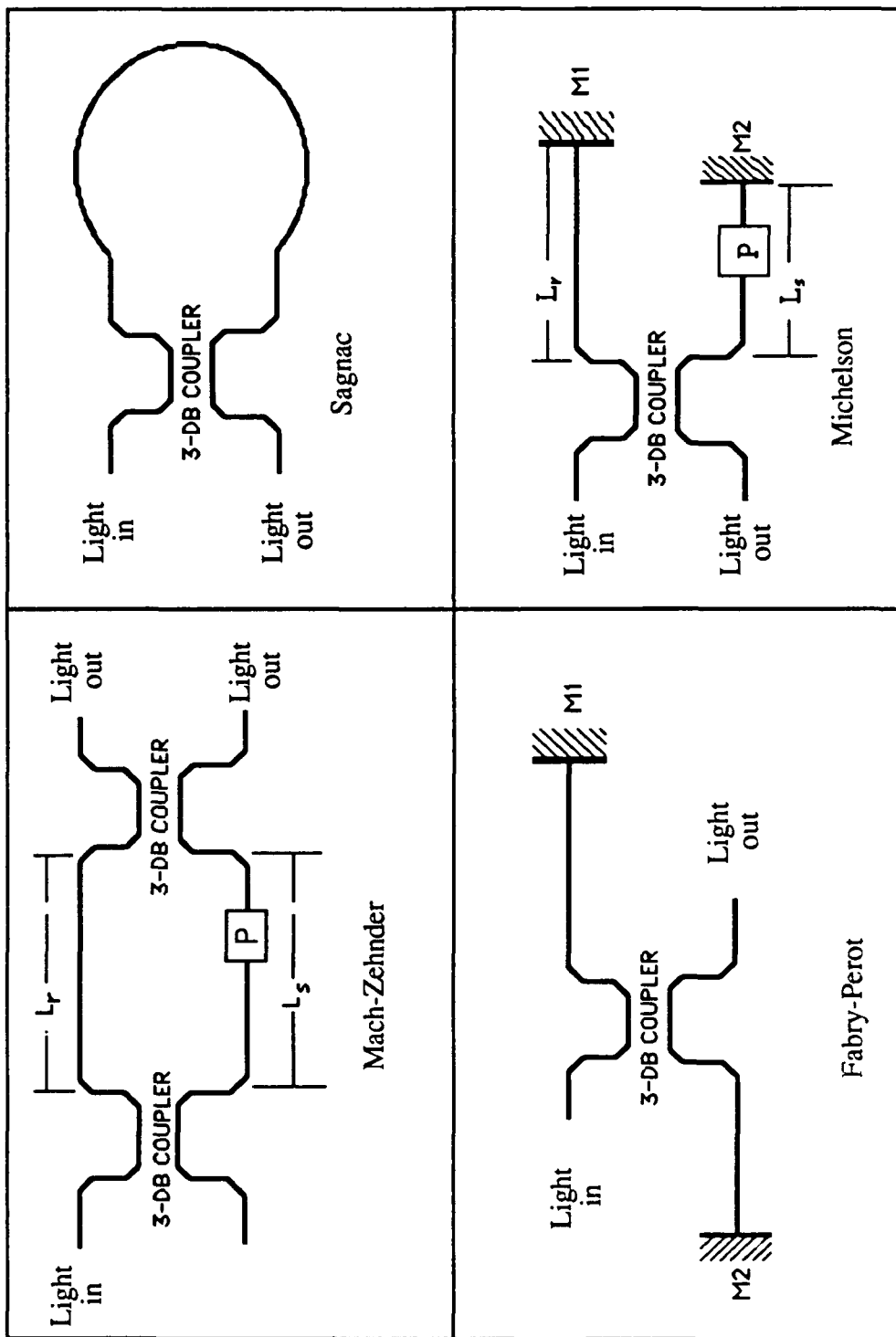Fig. 2 illustrates four popular fiber configurations of the classical interferometers.

Fig. 2. Four Popular Classical Interferometers

Fiber optic interferometers have reported detection capabilities of phase differences on the order of nuclear dimensions. Detection of phase shifts equivalent to a displacement of 10^{-13} meters (i.e., on the order or 1 μ radian) [13] were reported for a Mach-Zehnder fiber optic interferometer. A fiber optic resonator-type interferometer [14] has been reported that detects optical phase shifts on the order of 0.2 μ radian. Unfortunately, the higher sensitivities are accompanied by intrinsically poor measurand selectivity. Environmental noises due to the variability of the optical constants of the fiber (i.e., refractive index and length) produce a phase shift that is indistinguishable from phase shifts caused by desired measurand. The measurand sensitivity, particularly of the conventional Mach-Zehnder and the Michelson interferometers, is fixed and cannot be increased through parameter manipulation. Also, the environmental noise is not easily removed from the interferometer's output. Therefore, these standard configurations do not offer sensitivity enhancement.

2.1 The Conventional 1.0 Mach-Zehnder

Extensive investigation of numerous interferometer configurations as the basis of fiber sensor systems has been done, with the most successful approaches utilizing the conventional MZI and sophisticated signal processing to extract the phase information. The conventional Mach-Zehnder interferometric sensor will herein be referred to as the 1.0 MZI sensor to distinguish it from the 1.5 MZI sensor described in section 2.2. Fig. 3 is an optical schematic of a 1.0 MZI sensor. The performance of the 1.0 MZI is the benchmark against which other sensors are measured.
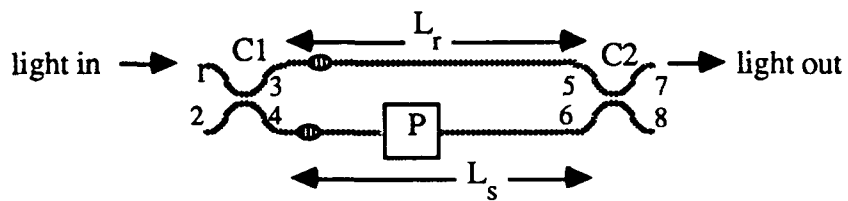
$$P = \frac{2\pi n_{eff}(L_r - L_s)}{\lambda} + \delta P_m$$

$$\tau = \frac{1}{2}(1 \pm \cos P)$$

$\oplus$ = splice

$\square$ = phase shifter(s)

━━━ = fiber

$\times$ = 3dB fiber coupler

Fig. 3. An Optical Schematic of a 1.0 MZI

A coherent optical source injects light into input port 1 of the 3-dB directional coupler, C_1. Input port 2 is unused. The directional coupler, C_1, divides the intensity equally between the two output ports 3 and 4. The light travels along the reference and the sensing paths. The reference path is isolated from the variations caused by the measurand while the sensing path is exposed to the measurand. In the sensing path, a phase modulator (e.g., a fiber stretcher [15]), P, provides a means to adjust the optical phase difference between the two paths, L_r and L_s, and simulate the measurand phase shift, δP_m. The two guided modes traversing the interferometers arms are coherently recombined in constructive or destructive interference depending on their relative phase at the input ports 5 and 6 of the 3-dB directional coupler, C_2. Ports 7 and 8, the output ports of the sensor, provide optical signals to detectors. A plot of the transmittance (sensor's output), τ, as a function of the phase is shown in Fig. 4. Note that the transmittance has a periodicity of 2π radians. This is significant because the transmittance is not a unique function of the phase, implying that a means to determine and keep track of the operating point is required.

2.2. The 1.5 Mach-Zehnder Sensor

The 1.5 MZI, so named for its resemblance to a 1.0 MZI cascaded to half of a 1.0 MZI, uses two different interference circuits that share a common directional coupler. An optical schematic is illustrated in Fig. 5. The 1.5 MZI sensor is a configuration introduced by Buckman, Pritchett, and Park [16]. The significance of this configuration is its "common-mode" (spatially uniform over the entire sensor) noise rejection and high measurand sensitivity without requiring an extremely coherent
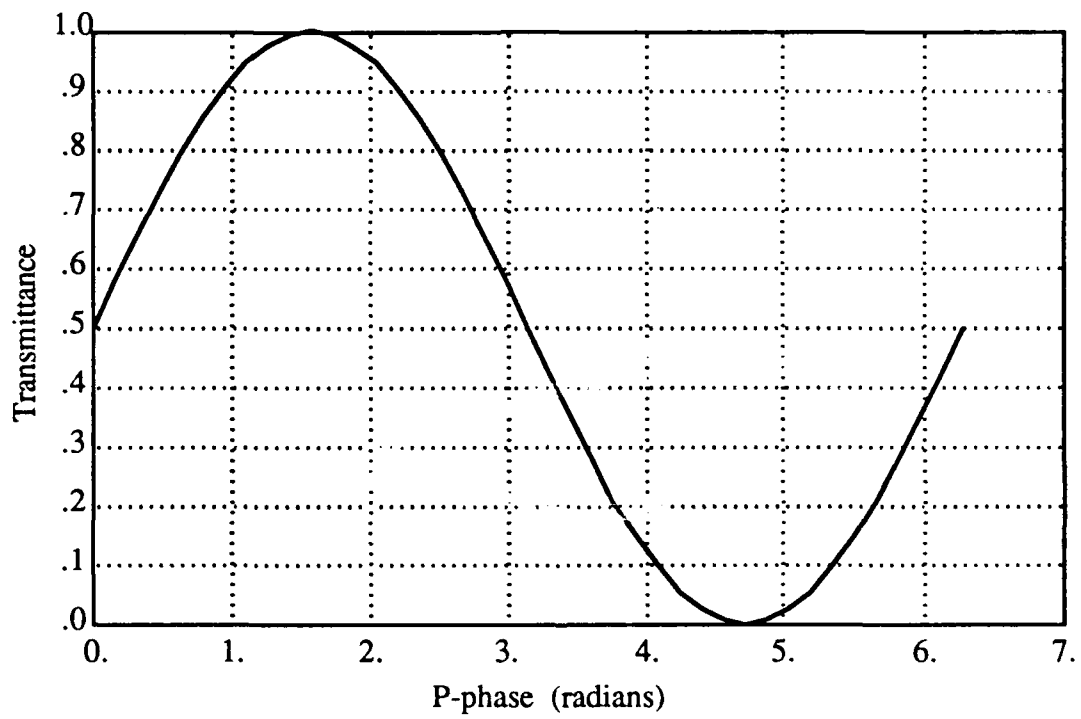
Fig. 4. Transmittance vs. Phase for a 1.0 MZI

$$\phi = \phi_0 \qquad\qquad P = P_0 + \delta P_m$$

$$\phi_0 = \frac{2\pi n_{eff}(L_a - L_b)}{\lambda} \qquad\qquad P_0 = \frac{2\pi n_{eff}(L_r - L_s)}{\lambda}$$

$$\tau = \frac{1}{2}(1 \pm \sin\phi \sin P)$$

$\oplus$ = splice

$\square$ = phase shifter(s)

$\rule{1cm}{0.4pt}$ = fiber

$\asymp$ = 3dB fiber coupler
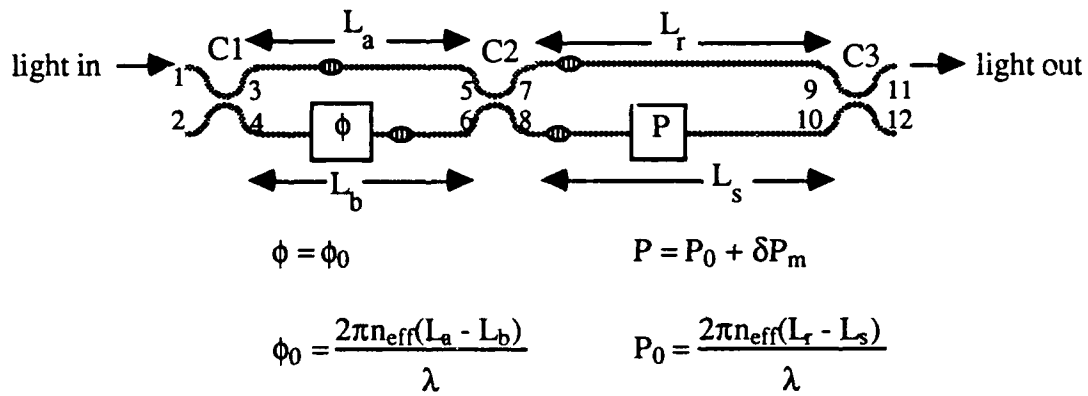
Fig. 5. An Optical Schematic of a 1.5 MZI

optical source and inordinately low coupler losses[17]. The interference circuits sense the measurand and control the common-mode noise rejection. Henceforth, they will be referred to as the sensing circuit and the compensating circuit, respectively. The sensing circuit has its phase altered in response to the measurand. The compensating circuit, located between the optical source and the sensing circuit, minimizes the measurement errors due to the random changes in the optical path differences. These random changes result from undesired physical displacement or variation in the optical constants of the fiber such as variations due to temperature or pressure changes.

Light enters the compensating circuit at port 1 of the 3-dB coupler, C_1. It divides equally between ports 3 and 4. A phase modulator, 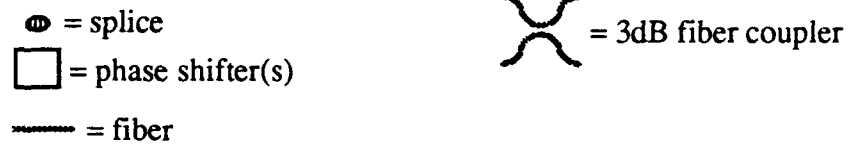ϕ, adjusts the phase of the sensing arm, thus regulating the phase bias between arms L_a and L_b of the compensating circuit. The light at ports 5 and 6 recombines in interference at C_2, a 3-dB coupler. Then it enters the sensing circuit being split between ports 7 and 8. A phase shifter, P, in the signal arm, L_s, of the sensing circuit regulates the phase bias between the two optical paths, L_r and L_s. ϕ_0 and P_0 are the optical phase shifts due to the path length differences. As the light incident on ports 9 and 10 interferes in the 3-dB coupler, C_3, the combined phase modulation of the sensing circuit and the compensating circuit is transmitted as an intensity variation to optical detectors at ports 11 and/or 12. An appropriate demodulation scheme is utilized to recapture the original phase modulated signal.

A graph of transmittance versus phase bias is illustrated in Fig. 6. This graph demonstrates how transmittance is a function of the sensing circuit phase bias, P, and compensating circuit phase bias, ϕ. Note that ϕ controls the amplitude of the transmittance. Fig. 7 is a graph of the measurand sensitivity (the sensor's ability to
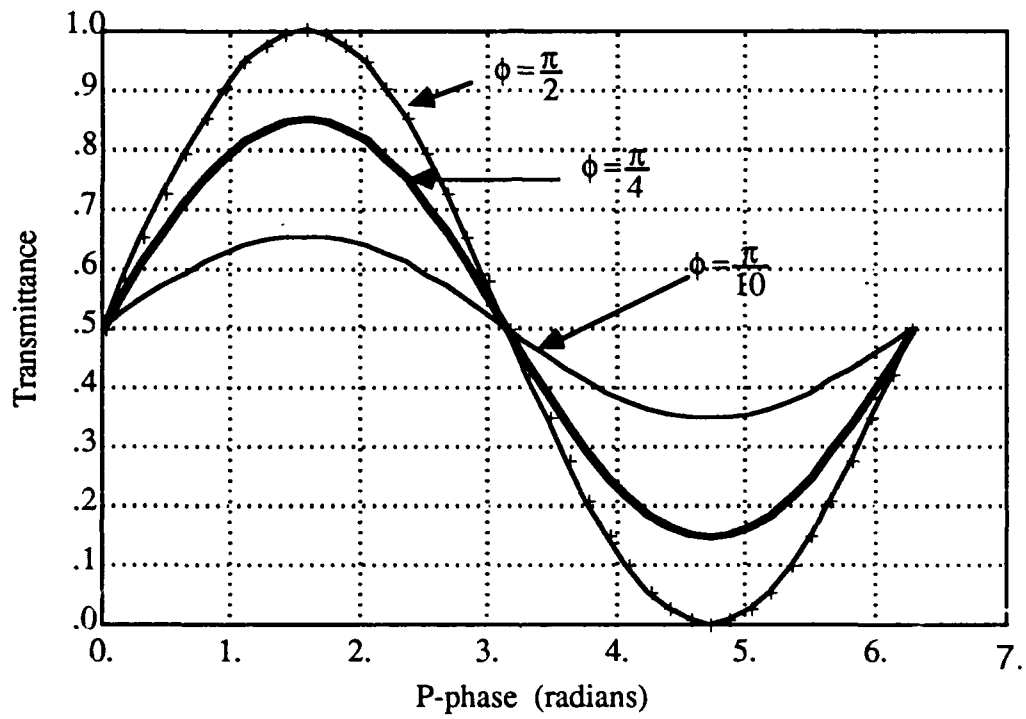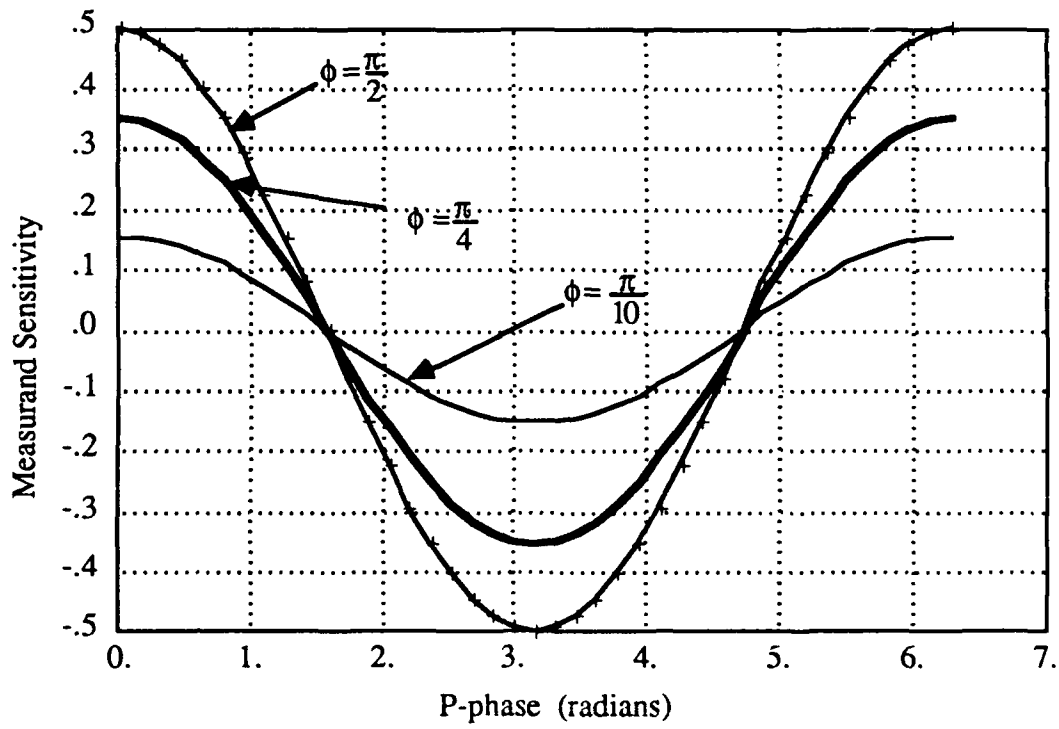
Fig. 6. Transmittance vs. Sensing Circuit Phase Bias

Fig. 7. Measurand Sensitivity vs. Sensing Circuit Phase Bias

sense the measured quantity) versus the sensing circuit phase bias, σ_m verses P, with

ϕ fixed at different values. Note how the amplitude of the measurand sensitivity changes for different values of ϕ. It achieves maximum sensitivity at $\phi = \frac{\pi}{2}$.

Chapter 3

Common-mode Compensation

The output of the interferometric sensor is a transmittance which depends on phase changes induced by the environment and the measurand. The changes due to the measurand are desirable; however, the changes caused by the environment are usually unwanted. The environmental noise (unwanted changes) may be categorized as common-mode and non-common-mode. Suppression of the common-mode (i.e., spatially uniform in all paths of the optical circuit) noise is the subject of this chapter, and non-common-mode noise will be examined in Chapter 5. Examples of common-mode disturbances are the drift of the center wavelength of the light source or a homogeneous pressure variation across the FOS circuit. Buckman, Pritchett, and Park [18] have demonstrated a method to minimize or eliminate the effects of common-mode noise from the output of the FOS. Using the method termed "common-mode compensation", Buckman [19] showed that the addition of an optical circuit to conventional fiber sensors allowed common-mode compensation (CMC) at phase biases corresponding to high measurand sensitivity. A detailed theoretical analysis and experimental results are presented in ref. [20]; therefore, only the essential points are presented below. To better understand how CMC is achieved, the measurand and the environmental sensitivities of the FOS must be examined.

3.1. Measurand Sensitivity

Measurand sensitivity is the sensitivity of the output transmittance, τ, to small changes in the quantity being measured. For a 1.5 MZI with lossless fibers, splices, and 3-dB couplers, the transmittance is given by:

$$\tau = \frac{1}{2}[1 \pm \sin\phi \sin P] \tag{3.1}$$

where ϕ is the optical phase of the compensating circuit, and P is the optical phase of the sensing circuit. ϕ regulates the amplitude or fringe visibility (difference between the maximum and minimum) of the transmittance, and P establishes the operating point and follows the measurand. The sign in equation (3.1) is dependent upon which output is used. The optical phase shifts in Fig. 5 are given by:

$$\phi = \phi_0$$
$$P = P_0 + \delta P_m \tag{3.2}$$

where δP_m = phase change due to the measurand, and

$$\phi_0 = \frac{2\pi n_{eff}\Delta L_\phi}{\lambda} + \phi_{piezo}$$

$$\tag{3.3}$$

$$P_0 = \frac{2\pi n_{eff}\Delta L_p}{\lambda} + P_{piezo}$$

where n_{eff} = fiber's effective index of refraction

ΔL_ϕ = path difference in compensating loop

ΔL_p = path difference in sensing loop

ϕ_{piezo} = phase bias added by voltage on ϕ-piezo (phase shifter)

P_{piezo} = phase bias added by voltage on p-piezo (phase shifter)

λ = wavelength of light source

ϕ_0 and P_0 are the operating points, called "phase biases," of the compensating and sensing circuits, respectively. They are adjusted by the optical path differences and the bias voltages applied to the piezos in their respective circuits.

Mathematically, the measurand sensitivity is obtained by differentiating the transmittance given in (3.1) with respect to the measurand, m.

$$\sigma_m = \frac{\partial \tau \, \partial P}{\partial P \, \partial m}$$

$$= \frac{1}{2} \sin \phi \cos P \frac{\partial P}{\partial m} \tag{3.4}$$

For the small signals of interest, P changes in direct proportion to the measurand. Therefore, to maximize measurand sensitivity, the phase biases must be adjusted to maximize the multiplicative factor

$$\frac{1}{2} \sin \phi \cos P$$

This factor can be maximized if the phase biases are adjusted so that

$$\phi = (2n + 1)\frac{\pi}{2}$$

$$P = n\pi \qquad n = 0, 1, 2,... \tag{3.5}$$

3.2. Environmental Sensitivity

Environmental sensitivity is the sensitivity of the output transmittance to physical parameters other than the measurand such as environmental pressures, source wavelength drift, and/or mechanical stresses. The effect of these perturbations on transmittance is described mathematically by taking the derivative of the transmittance with respect to the perturbed environmental variable:

$$\sigma_v = \frac{\partial \tau}{\partial v}$$

$$= \frac{\partial \tau \partial \phi}{\partial \phi \partial v} + \frac{\partial \tau \partial P}{\partial P \partial v} \tag{3.6}$$

v = perturbed environmental variable (i.e., n_{eff}, L, λ,...)

This equation includes only the dominant terms which depend on wavelength and optical path length differences. Other terms that depend on attenuation due to reflectivity and transmissive losses are considered negligible because typical lengths used in these FOSs are less than ten meters, and the decrease in intensity over such short lengths is extremely small. By taking the derivative of the transmittance (3.1) with respect to n_{eff}, L, or λ, the environmental sensitivity is shown to be:

$$\frac{\partial \tau}{\partial v} = \frac{2\pi}{\lambda}[\Delta L_\phi \cos \phi \sin P + \Delta L_p \sin \phi \cos P] \left[\frac{\partial n_{eff}}{\partial v} + n_{eff} \frac{1}{L} \frac{\partial L}{\partial v}\right] \tag{3.7}$$

In order to minimize the environmental sensitivity, $\frac{\partial \tau}{\partial v}$ must approach zero. This is accomplished if the phases, ϕ and P, and/or the path length differences, ΔL_ϕ and ΔL_p, are chosen such that

$$[\Delta L_\phi \cos \phi \sin P + \Delta L_p \sin \phi \cos P] \Rightarrow 0 \tag{3.8}$$

From equation (3.8), it seems apparent that the environmental effects can be eliminated by achieving zero path length difference (i.e., $\Delta L_\phi = \Delta L_p = 0$). It can be shown that this, however, results in the elimination of measurand sensitivity as well. Matching the path lengths to w⁺⁺ ᵢ ⱼ mm of each other is done in an effort to reduce the overall environmental efie ᵤ. This minute difference is still large enough to permit much of the common mode noise to pass through the system. Buckman, Pritchett, and Park [21] demonstrated that by adjusting the phase biases and the ratio of the path length differences, at least two points on the transmittance vs. sensing circuit phase (P-phase) curve becomes independent of small environmental effects which are spatially uniform over the entire sensor (i.e., common-mode noises)

An infinite number of values for ϕ and P will satisfy equation (3.8) as shown in Fig. 8, a graph of environmental sensitivity versus the sensing circuit phase bias, σ_v vs. P, at different values of ϕ. Adjusting the path length ratio moves the points where ϕ and P satisfy this condition and further increases the number of solutions for (3.8). The condition for maximum measurand sensitivity ($\phi=0.5\pi$ and P=0 or 2π) does not satisfy the condition for minimizing environmental sensitivity. Optimum phase biases must be appropriately selected to minimize environmental sensitivity and,
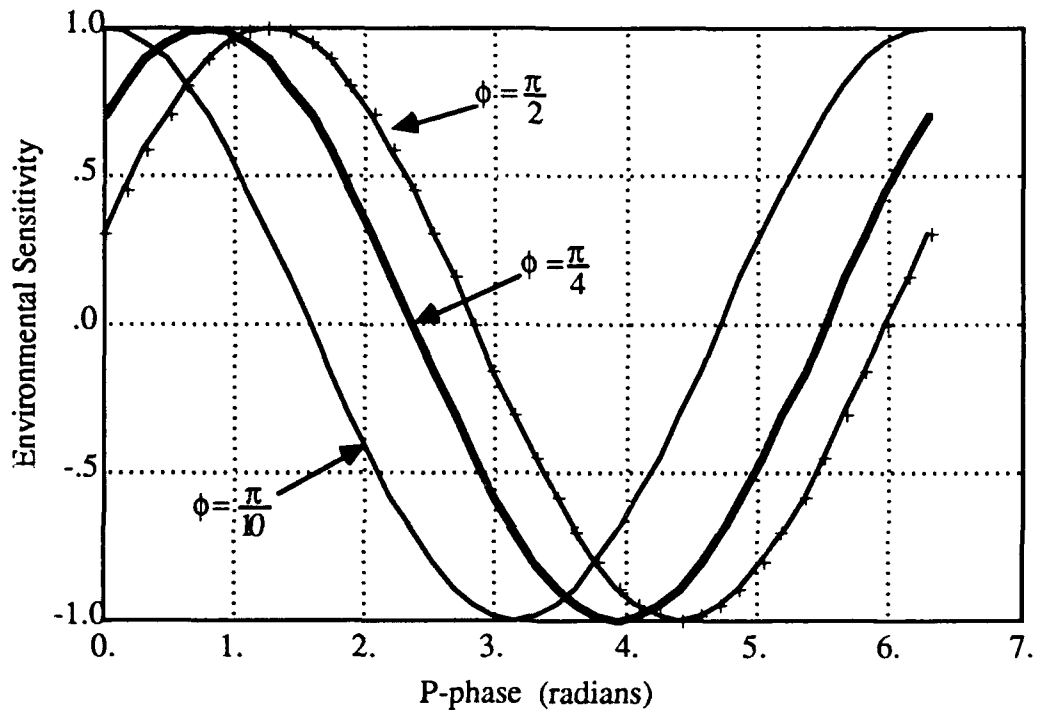
Fig. 8. Environmental Sensitivity vs. Sensing Circuit Phase Bias

simultaneously, maximize measurand sensitivity. The method to accomplish this is referred to as common-mode compensation.

3.3 Common-mode Compensation (CMC)

The principle used to achieve CMC is relatively simple. The compensating circuit is connected between the light source and the sensing circuit where it is only perturbed by the environmental fluctuations. Meanwhile, the sensing circuit is exposed to the environmental and measurand variations. Through adjustment of phase biases, the environmental disturbances in each circuit are made to oppose each other. The output of each circuit is combined such that the common-mode effects are minimized while leaving the effects due to the measurand perturbations essentially unchanged. Mathematically, the CMC condition is:

$$F_{cmc} = \frac{\partial \tau}{\partial \phi}\bigg|_{\phi_{cmc}} \left[N + \frac{\phi_{cmc}}{2\pi}\right] + \frac{\partial \tau}{\partial P}\bigg|_{P_{cmc}} \left[M + \frac{P_{cmc}}{2\pi}\right] = 0 \tag{3.9}$$

where "cmc" implies the common-mode compensated operating point and the bracketed terms are the path length differences, ΔL_ϕ and ΔL_P, converted to wavelengths. N and M are large integers. Because $\frac{\partial \tau}{\partial \phi}$ and $\frac{\partial \tau}{\partial P}$ exhibit enormous sensitivity to small changes in ϕ and P, the first and second terms of (3.10) are easily adjusted to become equal and opposite .

CMC reduces slightly the maximum measurand sensitivity achievable without enhancement. This sensitivity can be restored and further increased through electro-
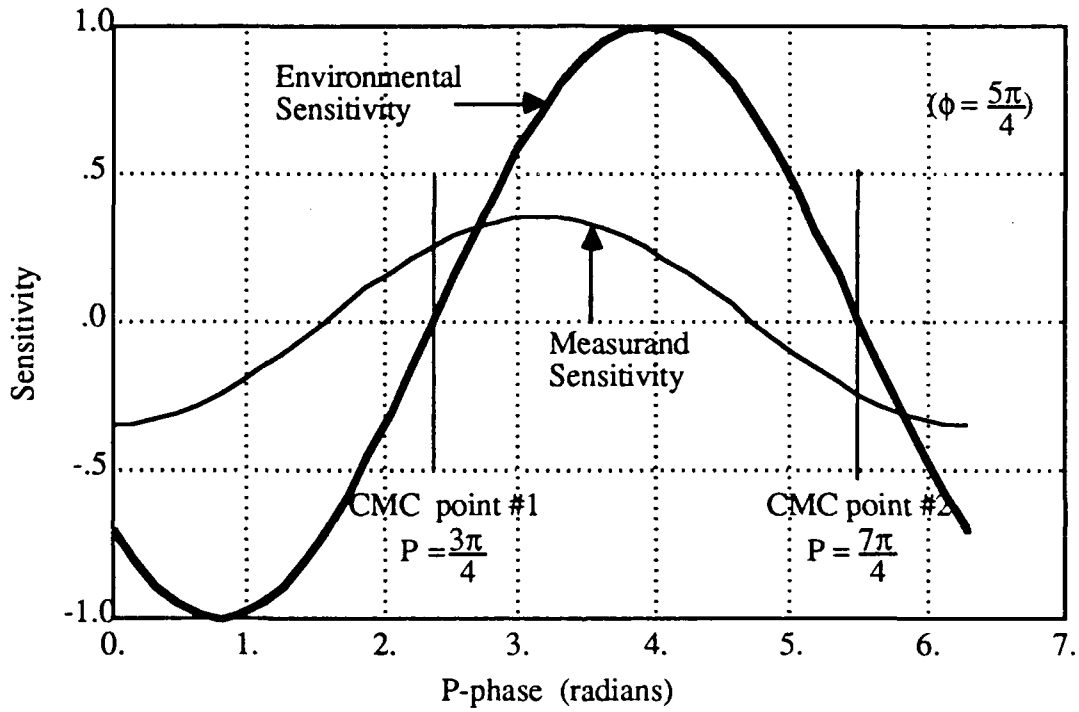
Fig. 9. Measurand and Environmental Sensitivity vs. Sensing Circuit Phase
Bias (CMC achieved)

optic feedback as will be discussed in the next chapter. Fig. 9 illustrates how CMC is accomplished through proper phase bias adjustment. Note how the measurand sensitivity is near a maximum when environmental sensitivity is zero. Fig. 10 depicts an example of how other than optimum phase biasing (ϕ set to $\frac{\pi}{2}$) affects the measurand sensitivity at the CMC point. Here the measurand sensitivity is zero when the environmental sensitivity is zero. A si ilated transmittance curve with a laser wavelength dither (common-mode noise) superimposed upon it is displayed in Fig. 11, for $\phi = \frac{5\pi}{4}$. Clearly visible are the regions of common-mode compensation (areas of the curve where the dither goes to zero).
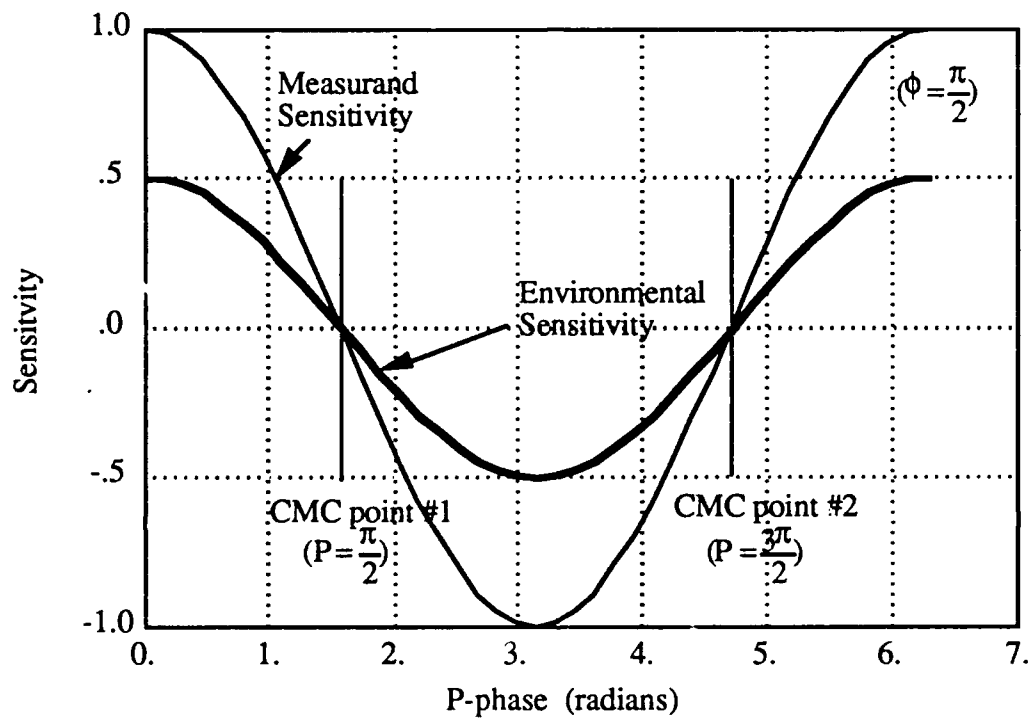
Fig. 10. Measurand and Environmental Sensitivity vs. Sensing
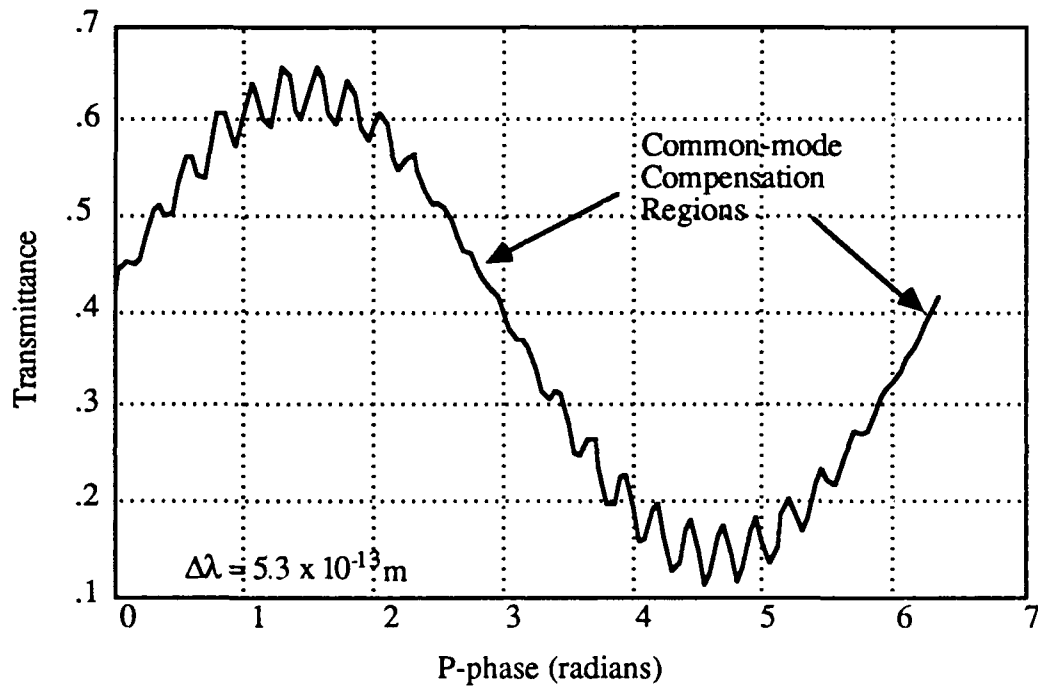Circuit Phase Bias (CMC not achieved)

Fig. 11. Transmittance vs. P with a Wavelength Dither of
Amplitude $\Delta\lambda$

Chapter 4
Enhanced Sensitivity

Buckman, Pritchett, and Park [22] demonstrated a novel concept to enhance the sensitivity of a Mach-Zehnder interferometric sensor an order of magnitude beyond the conventional Mach-Zehnder sensors by minimizing common-mode effects and utilizing electro-optic feedback (EOF). The minimization of common-mode effects was examined in the previous chapter. Here the effects of EOF are summarized. Since an extensive examination and experimental results were reported in ref. [23], a detailed theoretical analysis will not be presented. Instead, only the salient particulars are cited.

Using EOF to adjust the differential phase shifts in an interferometric FOS has been well documented. An active feedback loop employing a piezoelectric device was used to maintain constant phase quadrature and eliminate signal fading [24]. Another approach using DC power supplies and PZT cylinders was utilized to keep a Mach-Zehnder [25] and a Recirculating Delay Line FOS [26] biased in the regions of maximum sensitivity. Fig. 12 illustrates how EOF causes non-linearities in the transmittance versus measurand (P-phase) curve which greatly increases the sensitivity to small changes in the measurand over particular regions of the curve. Note how the slope of the curves changes with increasing feedback gain K.

A schematic of an enhanced sensitivity, CMC 1.5 MZI with EOF is shown in Fig. 13. The output intensity of the interferometer is detected and converted to a transmittance by the ratio network (division circuit). Then the interferometer's transmittance is fed back through an amplifier and added to the phase bias in the sensing circuit. This EOF is an added phase shift in P which is linearly proportional to
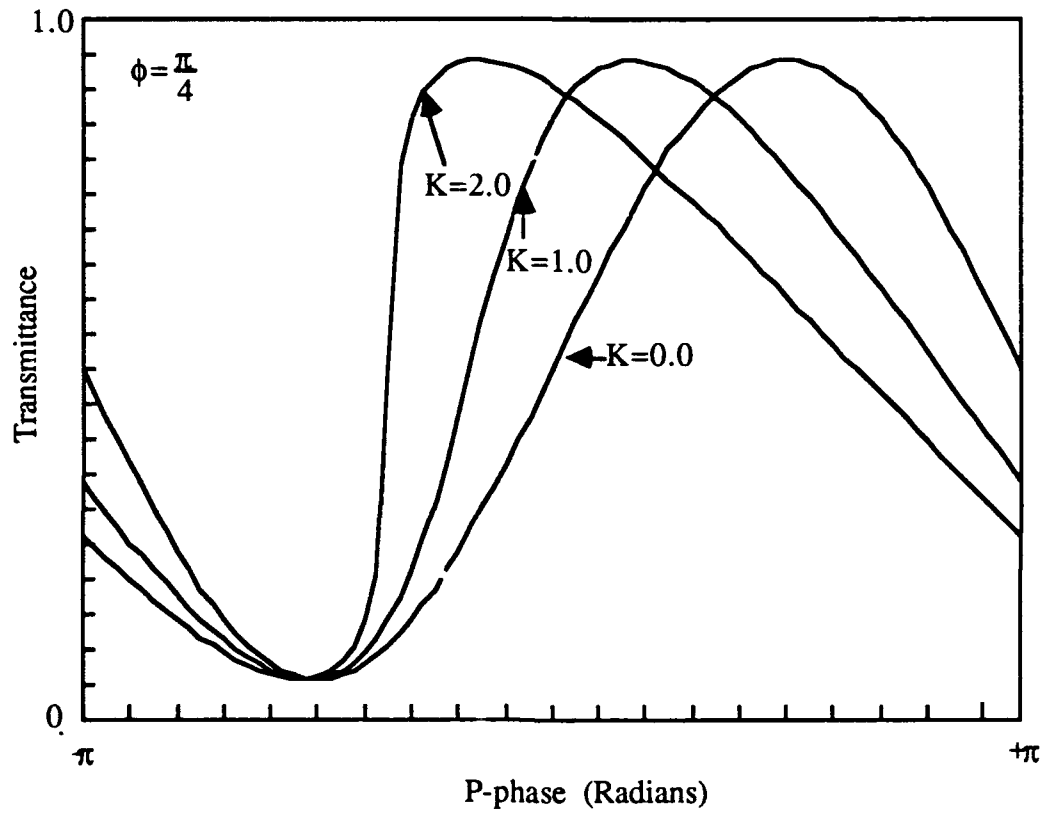
Fig. 12. Transmittance vs. Sensing Circuit Phase with EOF
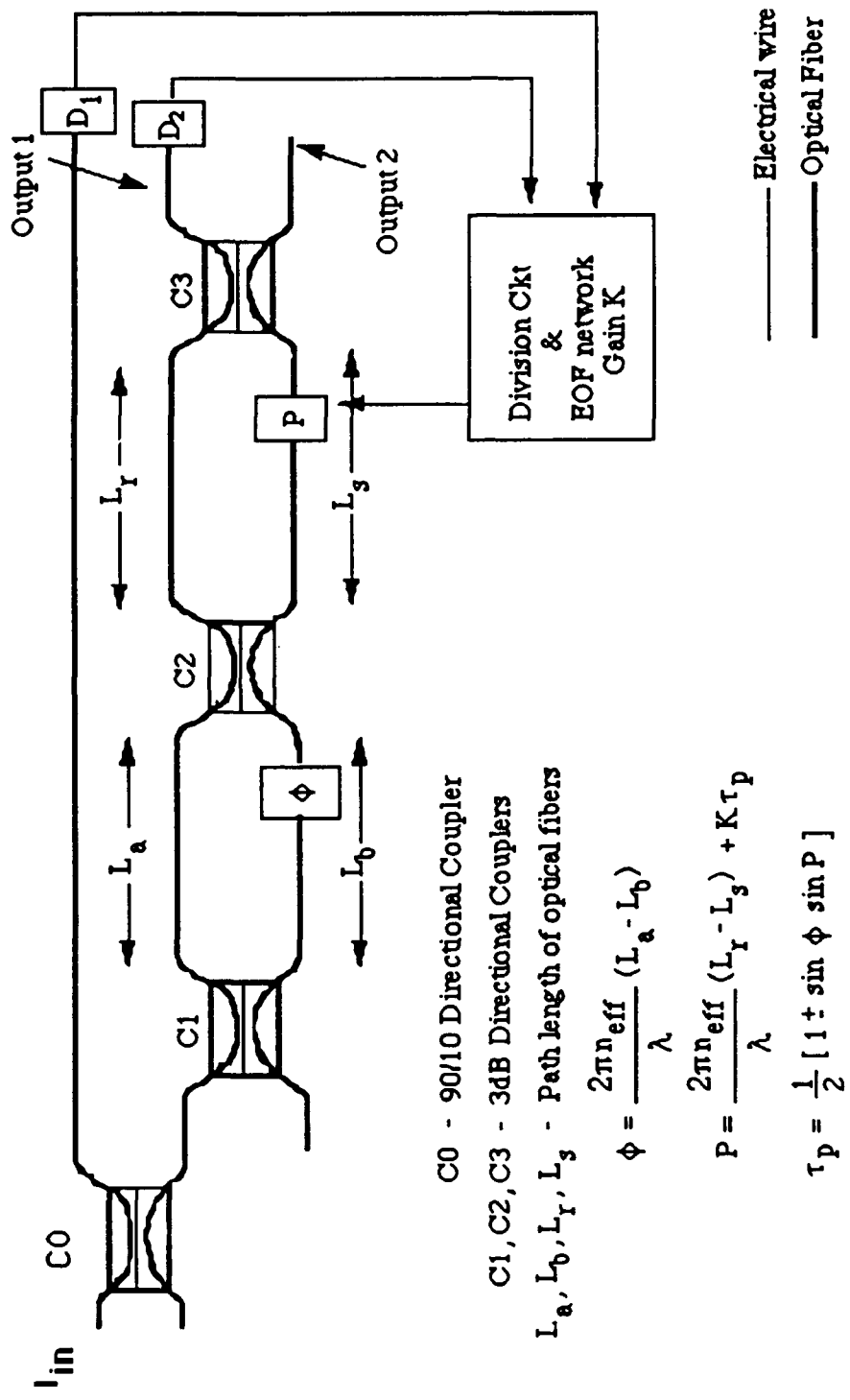
CO - 90/10 Directional Coupler

C1, C2, C3 - 3dB Directional Couplers

L_a, L_b, L_r, L_s - Path length of optical fibers

$$\phi = \frac{2\pi n_{eff}}{\lambda} (L_a - L_b)$$

$$P = \frac{2\pi n_{eff}}{\lambda} (L_r - L_s) + K\tau_p$$

$$\tau_p = \frac{1}{2} [1 \pm \sin \phi \sin P]$$

I_{in}

CO

C1

C2

C3

L_a

L_b

L_r

L_s

ϕ

P

D_1

D_2

Output 1

Output 2

Division Ckt & EOF network Gain K

—— Electrical wire
—— Optical Fiber

Fig. 13. Schematic of the 1.5 Mach-Zehnder sensor with feedback

the output transmittance of the interferometer. Neglecting coupler and splice losses, the transmittance remains as defined in equation (3.1):

$$\tau = \frac{1}{2}[1 \pm \sin\phi \sin P]$$

(4.1)

where

$$\phi = \phi_0$$

(4.2)

and

$$P = P_0 + K\tau$$

(4.3)

When equations (4.2) and (4.3) are substituted into equation (4.1), a transcendental equation in τ results.

$$\tau = f(\phi, P, K, \tau)$$

(4.4)

The solution to this equation was found numerically using a bisection algorithm [27]. Using (4.4), the measurand sensitivity of the sensor can be described by:

$$\sigma_m = \frac{\partial\tau}{\partial m}$$

$$= \frac{f(\phi, P, K, \tau)}{1 - Kf(\phi, P, K, \tau)}$$

(4.5)

It is easily seen in (4.5) how adjusting K, the feedback gain, affects the measurand sensitivity. Less obvious from (4.5) is the effect that the value of ϕ has on the

measurand sensitivity. However, it was pointed out in Chapter 3 how ϕ regulates the fringe visibility of the transmittance and affects the amplitude of the measurand sensitivity. Fig. 14 reveals further the effects of ϕ and EOF on the sensor's transmittance. These effects translate into changes affecting the sensor's measurand sensitivity.

In order to insure the sensor's operation in the region of highest sensitivity, some means of control must be incorporated to maintain accurately the phase biases, ϕ and P_0, and the EOF. The experiments of Buckman, Pritchett, and Park [28] did not incorporate an electronic/optical system for such control, but rather used the interferometer in a free-running mode to demonstrate the existence of high sensitivity regions with CMC. The research reported in this dissertation investigates the design and implementation of active control of the phase biases in a 1.5 MZI with EOF to achieve a reduced minimum detectable phase shift. This control system is described in the next chapter.
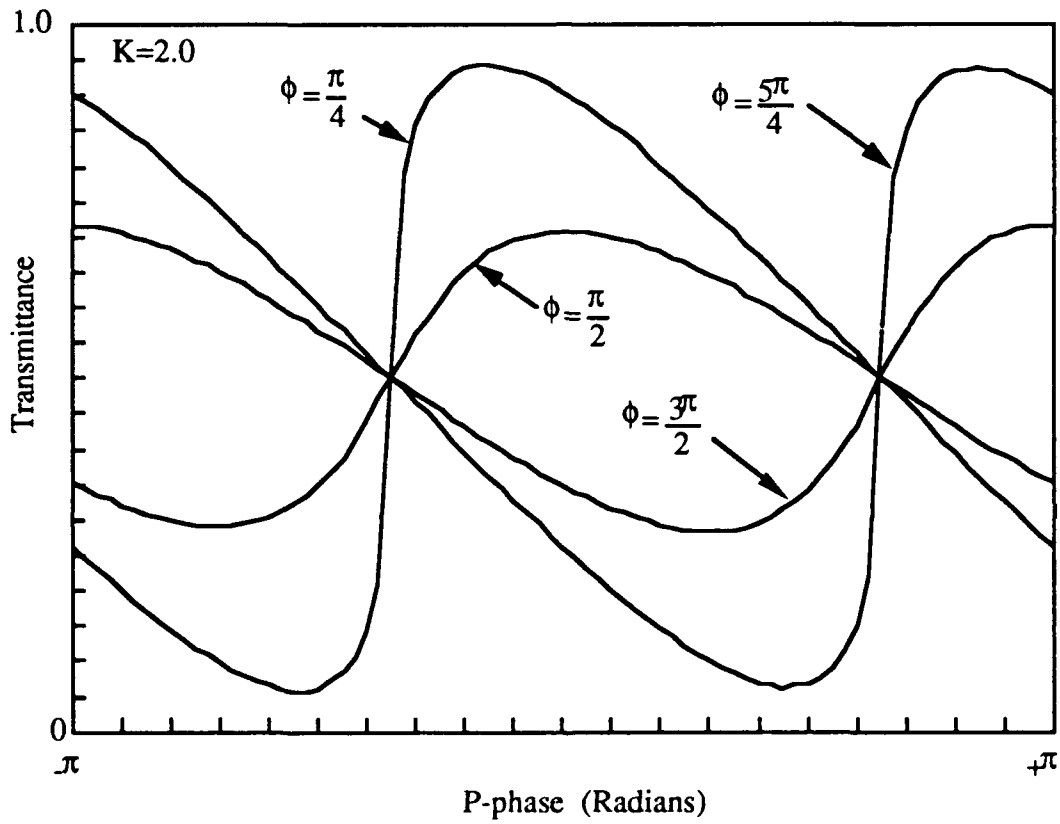
Fig. 14. Transmittance vs. Sensing Circuit Phase with EOF and
Different Values for the Compensating Circuit Phase Bias

Chapter 5
The Controller

The very property which makes fiber optic interferometric sensors so appealing, their extraordinary sensitivity, also makes them extremely vulnerable to random (non-common-mode) environmental changes. Temperature variations can induce relatively large phase shifts. Pressure gradients and air currents can limit the phase shift detectability by creating low frequency (<100 Hz) drifts in the sensor's output which are indistinguishable from measurand perturbations. For interferometric sensors manufactured from non-polarization preserving fiber, signal fading caused by differential drift can degrade the amplitude of the detected signal to zero [29]. In order to achieve the maximum sensitivity and linearity in the presence of differential phase modulation caused by environmental disturbances (temperature, pressure, wavelength drift, etc.), the sensor's operating point must be stabilized. Measurement techniques employing active (with feedback) [30] and passive (no feedback) [31] detection schemes have been contrived to maintain the interferometric sensor's maximum output signal. The controller described in this chapter is an active stabilization circuit that maintains the operation of an ES-CMC 1.5 MZI [32] over the narrow operating range required for common-mode compensation and high sensitivity. This control system can be programmed to track the low frequency variations and maintain the correct operating point.

5.1. Principle of Operation

The schematic of the complete FOS is illustrated in Fig. 15. It shows the optical circuit and the functional diagram of the controller electronics. The ES-CMC 1.5 MZI is configured to use two cascaded 1.0 MZIs, one as the compensating circuit and the other as the sensing circuit. In order to stabilize the FOS by implementing a phase-tracking approach, each interference circuit must be individually controlled at preset phase values employing feedback loops. The controller accomplishes this by applying a DC level and a pseudo common-mode dither to the phase modulators, ϕ and P, of the interferometer. The DC level causes the phase modulators to expand or contract as required to maintain a preselected optical phase difference between the arms of each circuit. This, in turn, maintains a particular operating point on the transmittance curves. However, due to the nonuniqueness of the sensor's transmittance as a function of the interference circuit phase (the sensor has a periodicity of 2π radians), multiple phase values correspond to each transmittance level. As illustrated in Fig. 16, a transmittance level of 0.7 corresponds to phases of 0.4 and 2.73 radians on the τ_ϕ transmittance curve. To eliminate the ambiguity of the transmittance-phase relationship, the pseudo-common-mode dither (henceforth, referred to as the dither), used in conjunction with a phase logic circuit within the controller, selects and maintains the correct phase bias for ϕ.
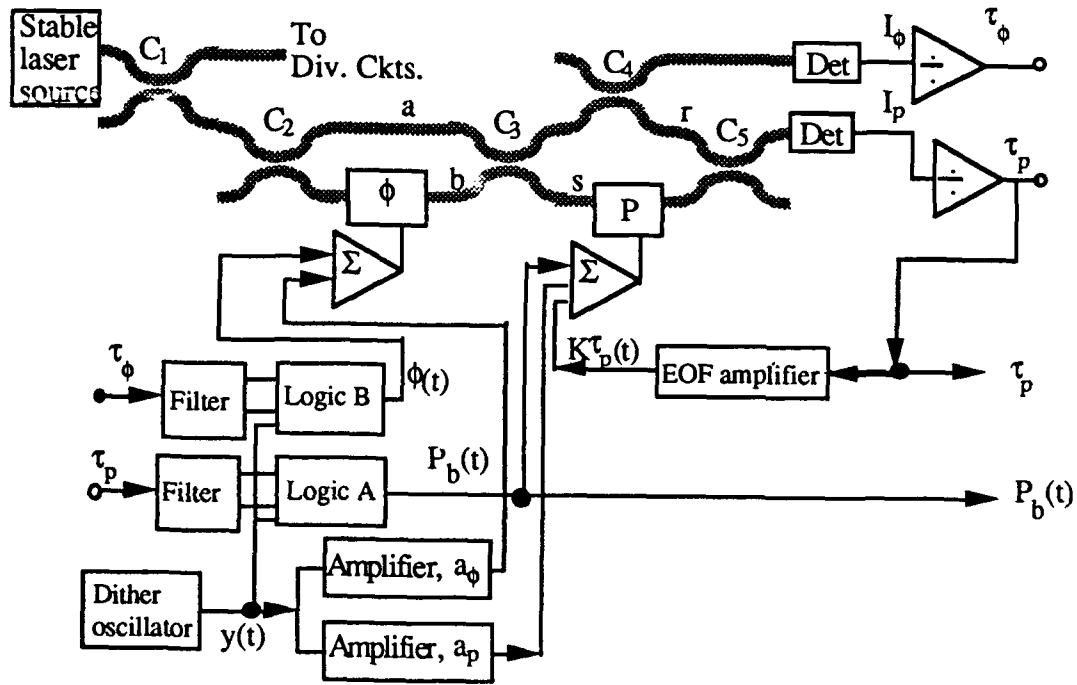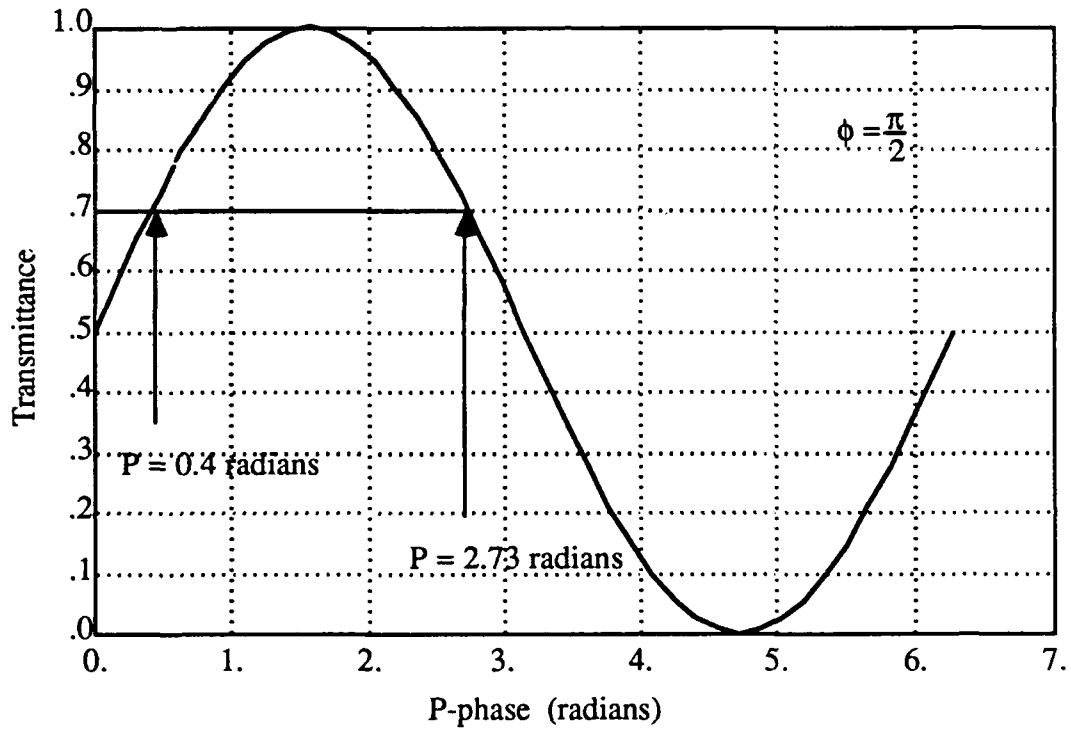
Fig. 15. Schematic of the Complete FOS System

Fig. 16. The Transmittance-Phase Relationship on τ_p

5.1.1. Stabilization of the Compensation Circuit.

The intensity variations of the compensating circuit, ϕ-loop, are detected from the ten percent arm of the directional coupler, C_4. The signal is then transformed into a transmittance at the output of the division circuit. The transmittance, τ_ϕ, is proportional to the transmittance of a 1.0 Mach-Zehnder given by:

$$\tau_\phi = \frac{1}{2}(1 \pm \cos \phi) \tag{5.1}$$

where

$$\phi = \frac{2\pi n_{eff}(L_a - L_b)}{\lambda}$$

If a dither signal, $a_\phi \sin(\omega_1 t)$, is imposed upon the ϕ phase modulator, the phase becomes

$$\phi(t) = \phi_b(t) + a_\phi \sin (\omega_1 t) \tag{5.2}$$

where

$$\phi_b = \frac{2\pi n_{eff}(L_a - L_b)}{\lambda}$$

Under the assumption that the amplitude of the dither signal, a_ϕ, is small, it can be shown by Taylor series expansion that the compensating circuit output transmittance can be approximated by the summation of its DC and fundamental dither frequency components:

$$\tau_\phi(t) = C [1 - \cos \phi(t)]$$
$$= C [1 - \cos \phi_b(t)] + C a_\phi \sin[\phi_b(t)] \sin(\omega_1 t) \tag{5.3}$$

where C is a constant of proportionality.

A system can be implemented that stabilizes the compensating circuit by separately acting on the DC and fundamental dither frequency components.

To track and hold the compensating circuit at a specific phase bias, ϕ_b, an error signal is produced and applied to the phase modulator as a correction signal. This error signal is the difference between the operational bias level (first term on the right of equation 5.3) and the desired bias level. It is integrated and fed back to the phase modulator. The direction of integration for the error signal integrator is determined by a phase logic unit in the controller. The logic unit compares the relative phases of the dithered transmittance (second term on the right side of equation 5.3) and the original dither to generate a control signal. The control signal maintains operation of the compensating circuit on the exact location of the desired phase bias. The direction of integration is changed according to the algorithm outlined in Table 2:

Table 2. Compensating Circuit Logic Unit Algorithm

Location of desired operating point relative to actual operating point (X_d =desired; X_0 = actual)	Relative phase of the dither and reference signals ($X_1 \cdot Y > 0 \Rightarrow$ positive slope; $X_1 \cdot Y < 0 \Rightarrow$ negative slope)	Direction controller will drive phase, ϕ_b, to reestablish desired operating point
$X_d - X_0 > \varepsilon$	$X_1 \cdot Y > 0$	increase ϕ_b
$X_d - X_0 < \varepsilon$	$X_1 \cdot Y > 0$	decrease ϕ_b
$X_d - X_0 < \varepsilon$	$X_1 \cdot Y < 0$	decrease ϕ_b
$X_d - X_0 > \varepsilon$	$X_1 \cdot Y < 0$	decrease ϕ_b
$|X_d - X_0| > \varepsilon$	$X_1 \cdot Y < 0$	decrease ϕ_b
$|X_d - X_0| > \varepsilon$	$X_1 \cdot Y > 0$	No action

The signals X_d, X_0, X_1 and Y in Table 2 are defined as

X_d = the desired operating point on τ_ϕ

X_0 = the actual operating point on τ_ϕ

X_1 = the transmittance component at the dither frequency

Y = the reference dither output

Fig. 17 shows graphically how the algorithm is implemented over the transmittance curve to maintain the correct phase operating point. Note that the operating point is held within a modulo value $\pm 2N\pi$ where N is an integer.

5.1.2. Stabilization of the Sensing Circuit.

Stabilizing the sensing circuit is procedurally similar to stabilizing the compensating circuit; however, an additional signal, the EOF, is applied to the P phase modulator. It is added at this point to enhance the overall interferometer sensitivity. The phase of the sensing circuit is given by:

$$P(t) = P_b(t) + a_P \sin(\omega_1 t) + K \tau_P(t) \qquad (5.4)$$

where

$$P_b = \frac{2\pi n_{eff}(L_T - L_S)}{\lambda}$$

Note that the phase P is a function of ϕ and K when feedback is added; thus, ϕ must be stabilized before the sensing circuit can be stabilized. The EOF gain coefficient, K. provides a non-linear effect that distorts one slope of the transmittance curve, thus producing a narrow dynamic range of greatly increased sensitivity. Since the signals of
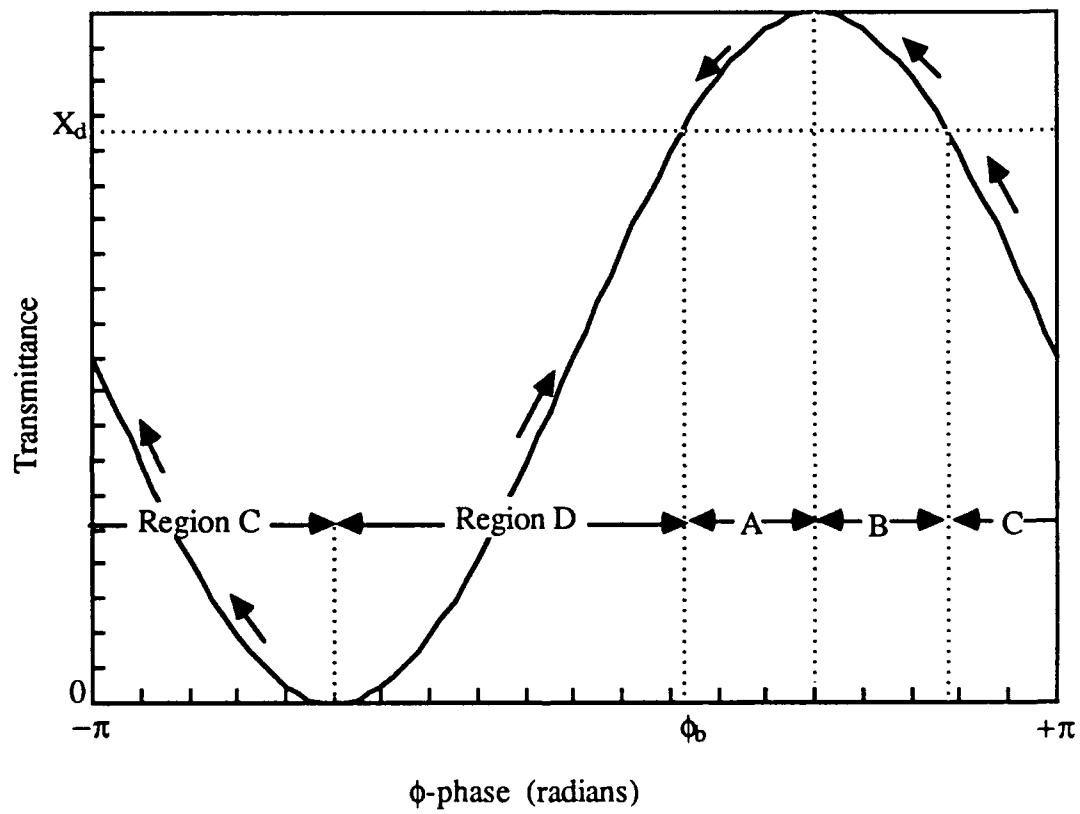
Fig. 17. The Implementation of the Compensating Circuit Bias
Control Algorithm over τ_ϕ

interest generate small measurand-induced phase shifts within this narrow dynamic range, no adverse effects on controlling the sensing circuit is encountered due to the EOF signal.

Assuming a small amplitude, a_p, for the sinusoidal dither ($a_p \sin(\omega_1 t)$) applied to the P phase modulator, the output transmittance can be approximated by the summation of its DC term and its first harmonic:

$$\tau_p(t) = \tau(P_b, \phi_b, K) + \frac{\partial \tau}{\partial P} \delta P$$
$$+ \{a_\phi \frac{\partial \tau}{\partial \phi} + a_p \frac{\partial \tau}{\partial P}\} \sin(\omega_1 t)$$

$$(5.5)$$

The measurand sensitivity, $\frac{\partial \tau}{\partial P}$, is large for the FOS; therefore the DC component (first two terms on the right side of equation (5.5)) is very sensitive to small phase shifts, δP. Biasing for common-mode compensation causes the dithered components (latter term on the right side of equation (5.5) having $\sin(\omega_1 t)$ as a factor) to be weakly sensitive to small phase shifts. Thus, as in the compensating circuit, a control scheme can be implemented that utilizes separately the DC and first harmonic frequency components. The phase logic unit compares the operating phase bias (DC component) to the desired operating bias and the phase of the dithered transmittance (first harmonic) to the phase of the original dither. Then it outputs a correction signal to the P phase modulator to maintain the correct bias according to the algorithm shown in Table 3. The signals T_d, T_0, T_1 and Y in Table 3 are defined as

T_d = the desired operating point on τ_p

T_0 = the actual operating point on τ_p

T_1 = the transmittance component at the dither frequency

Y = the reference dither output

Table 3. Sensing Circuit Logic Unit Algorithm

Location of desired operating point relative to actual operating point (T_d =desired; T_0 = actual)	Relative phase of the dither and reference signals ($T_1 \cdot Y > 0 \Rightarrow$positive phase; $T_1 \cdot Y < 0 \Rightarrow$negative phase)	Direction controller will drive phase, P_b, to reestablish desired operating point
$T_d - T_0 > 0$	$T_1 \cdot Y > 0$	decrease P_b
$T_d - T_0 < 0$	$T_1 \cdot Y > 0$	decrease P_b
$T_d - T_0 > 0$	$T_1 \cdot Y < 0$	increase P_b

Fig. 18 graphically illustrates how the algorithm is implemented over the transmittance curve to maintain the correct phase operating point. Again, note that the operating point is held within a modulo value $\pm 2N\pi$ where N is an integer. The sensing circuit and compensating circuit algorithms provide a means for the control circuitry to automatically locate and maintain the optimum phase biases for the FOS from power-up.

5.1.3. Maintaining Enhanced Sensitivity and Common-mode Compensation

The controller utilizes three feedback loops to maintain enhanced sensitivity and common-mode compensation. As stated earlier, the ϕ-loop controls fringe visibility of the transmittance output, the P-loop establishes the operating point, and the sensitivity
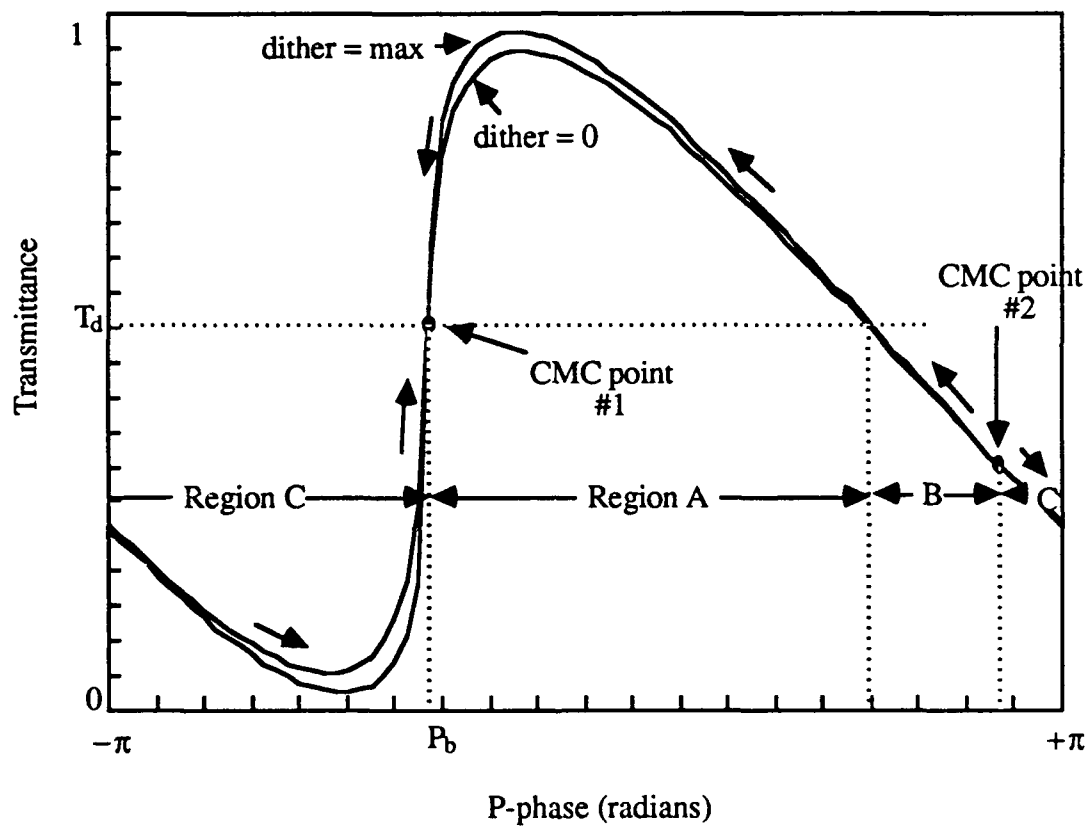
Fig. 18. The Implementation of the Sensing Circuit Bias
Control Algorithm over τ_p

loop nonlinearly deforms the transmittance curve to produce the narow regions of high measurand sensitivity. The responsivity of the sensor is dependent on the frequency response of each of these loops. Because the ϕ-loop is unaffected by the other loops and just controls the ϕ phase bias, it requires only sufficient speed to react to the slowly varying environmental changes affecting the compensating loop. Most of the environmental perturbations such as temperature and pressure induced variations are changing at frequencies less than 100 Hz; thus, the frequency response of the ϕ-loop need not be much greater.

The P-loop, like the ϕ-loop, must respond to the slowly varying environmental changes on the sensing circuit; and it must also react to the changes in its optimum operating point induced by the measurand. Generally, the measurand is of higher frequency content than the environmental changes. On the assumption that the measurand signal and environmental noises are separable in frequency, then it is possible to adjust the frequency response of the P-loop to compensate for the noise and permit a stable signal to be observed. The frequency response of the P-loop must be adjusted slightly above the frequency of the environmental noise or similar to the ϕ-loop. The low frequency noise will appear in the error correction signal applied to the phase modulator, thereby maintaining the optimum phase bias, P_b. The faster measurand changes will exceed the response of the feedback loop and appear as a change in the transmittance output. Any component of the measurand signal that does not exceed the response of the feedback loop will appear along with the noise in the correction signal. A technique to separate the noise from the desired signal would be necessary to recover the signal. An alternative for low frequency measurand signals is

frequency shifting. The low frequency signal can be shifted above the response of the feedback loop and an appropriate demodulation scheme utilized to recover the signal.

In order for the sensor to maintain its high sensitivity, the operating point of the measurand must be maintained in the narrow region of increased sensitivity. This can only be accomplished if the sensitivity loop's frequency response is greater than any measurand variations sensed by the FOS. This means that the sensitivity loop must have a bandwidth that encompasses the highest frequency for which the FOS is designed to measure. Therefore, the sensitivity loop establishes the upper frequency limit for the measurand. Fig. 19 shows the relative frequency response of the FOS outputs. The response labeled P_b is constrained by the time constant, τ_1, of the P-loop while the transmittance response is limited by the time constant of the sensitivity loop, τ_{EOF}. As indicated by the dip in the response curve, a narrow band of information in the vicinity of the dither frequency is unrecoverable. The dither frequency is used to control the appropriate phase biases to achieve common-mode compensation.

In order to employ active stabilization of a 1.5 MZI to achieve common-mode compensation, the phase biases of the sensing and compensating circuits must be regulated at predetermined values. This is accomplished by generating a "pseudo" common-mode signal and, then, adjusting the phase biases until it is nulled. By supplying a dither signal to the phase modulators that is proportional to the path length differences of each interference circuit, that is

$$\frac{a_p}{a_\phi} = \frac{L_s - L_r}{L_b - L_a}$$

(5.6)

the phase biases and feedback gain can be adjusted such that the dither vanishes when common-mode compensation is achieved. When the dithered component of the
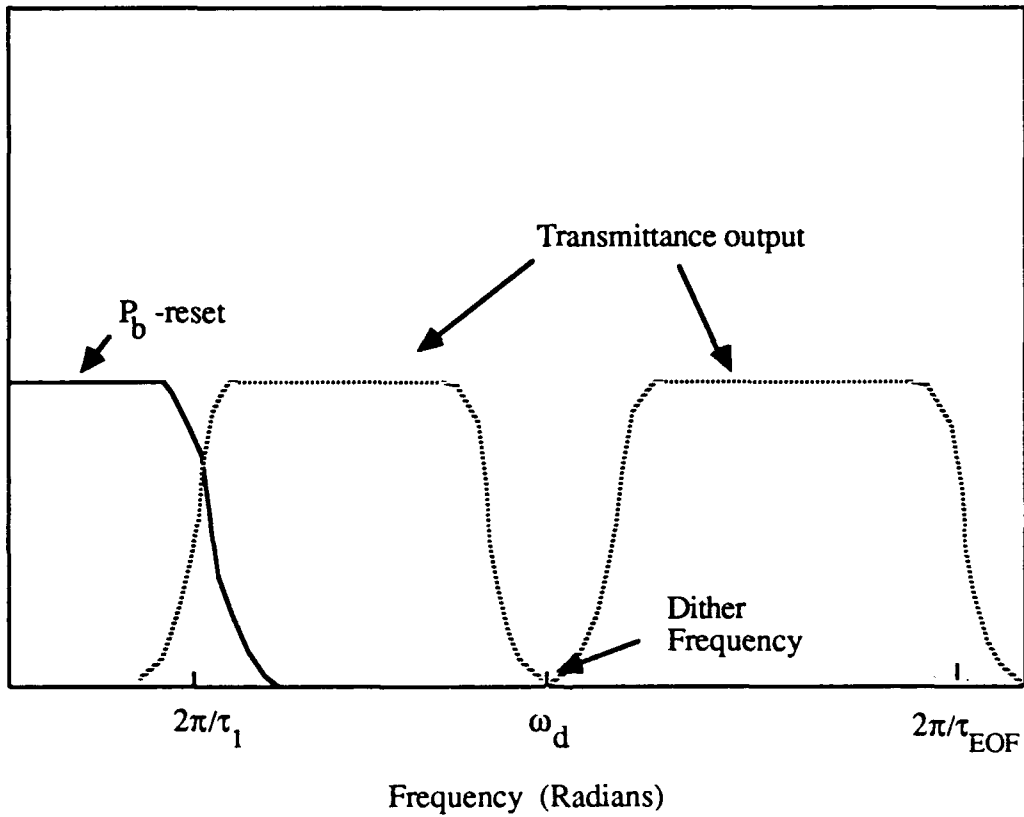
Fig. 19. Relative Frequency Response of the FOS Outputs

transmittance is non-zero, its phase relative to the original dither signal provides information to adjust the phase biases such that common-mode compensation point is reached. Fig. 20 shows a numerical simulation of the transmittance curves and the dither signal phase reversals. The dithered component of τ_ϕ reverses its phase and passes through zero about the maximum and minimum point of the compensating circuit transmittance. Likewise, the dithered component of τ_p reverses its phase and passes through zero about the common-mode compensation point. The control algorithms described earlier in this chapter are designed to utilize this information.

5.2. Circuit Description

The FOS system is divided into an optical and an electronic circuit as previously illustrated in Fig. 15, the schematic of the complete fiber optic sensor. Since the optical circuit is similar to the 1.5 MZI described in Chapter 2, only the differences are explained below. The operation of the controller electronics is described in detail.

5.2.1. Optical Circuit

The 1.5 MZI used in the experiment differs only slightly from the standard 1.5 MZI shown in Fig. 5. The optical schematic of Fig. 15 illustrates these differences. First, an optional 90/10 directional coupler, C_1, is inserted between the light source and C_2. Ninety percent of the light is coupled to the input of the sensor at C_2. The remaining ten percent of the source radiation is directed to two ratio networks as an optical reference level. Within the ratio networks, the output intensities, I_ϕ and I_p, are
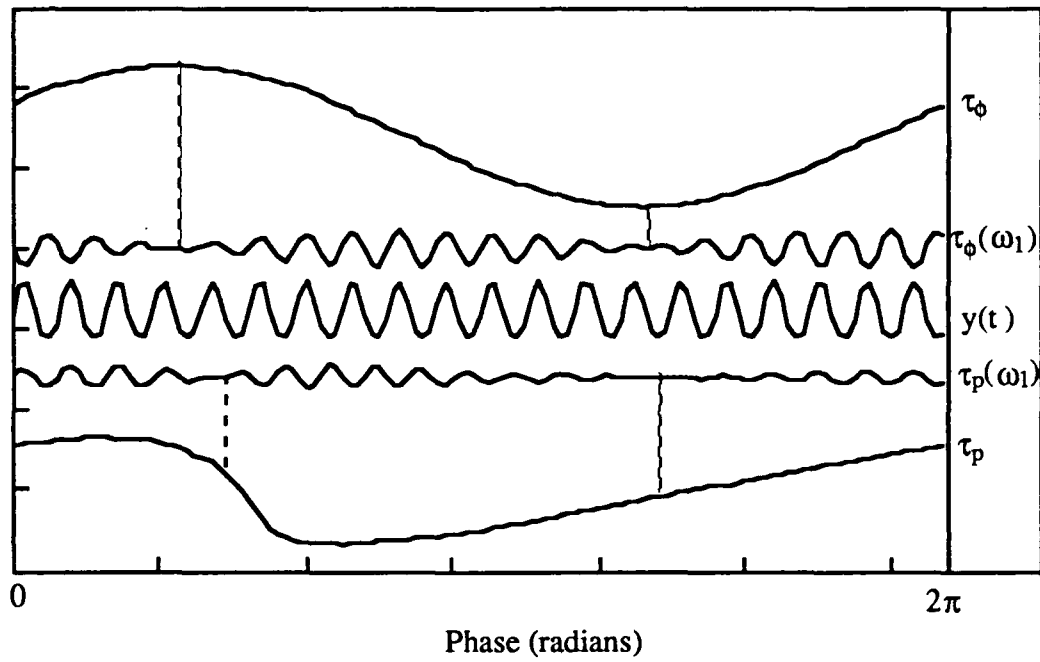
Fig. 20. Numerical Simulation of Transmittance Curves
and Dither Phase Reversal.

divided by the reference level to produce output transmittances, τ_ϕ and τ_p. The purpose of the ratio networks is to minimize the effects of the intensity fluctuations of the optical source. If the laser intensity is extremely stable over time, the requirement for the reference level is unnecessary; the output intensities can be used directly.

Second, in order to extract all of the necessary information to stabilize the 1.5 MZI, an additional optical tap was inserted after the directional coupler C_3. This tap allowed the compensating loop to be interrogated for the ϕ intensity variation. The tap was accomplished by inserting C_4, a 90/10 directional coupler after C_3. The ten percent of light coupled from the sensor, labeled I_ϕ in Fig. 15, is used to control the value of ϕ independent of P.

5.2.2. Controller Electronics

Figs. 21 and 22 are block diagrams of the controller electronics. Detailed schematics of the individual controller circuits are presented in the Appendix B. As shown in the block diagram, the controller is divided into two nearly identical sections utilizing a common dither and reference generator. The upper section controls the optical compensating circuit (ϕ-loop), and the lower section controls the optical sensing circuit (P-loop). Henceforth, these sections wil be referred to as the ϕ-controller and P-controller, respectively. Each section contains a low-pass filter, a narrow band-pass filter and phase shifter, a bias level comparator, a phase comparator, a phase logic circuit, an integrator, and a summing amplifier. The P-controller differs from the ϕ-controller only in its inclusion of a feedback amplification input to the summing amplifier for EOF.
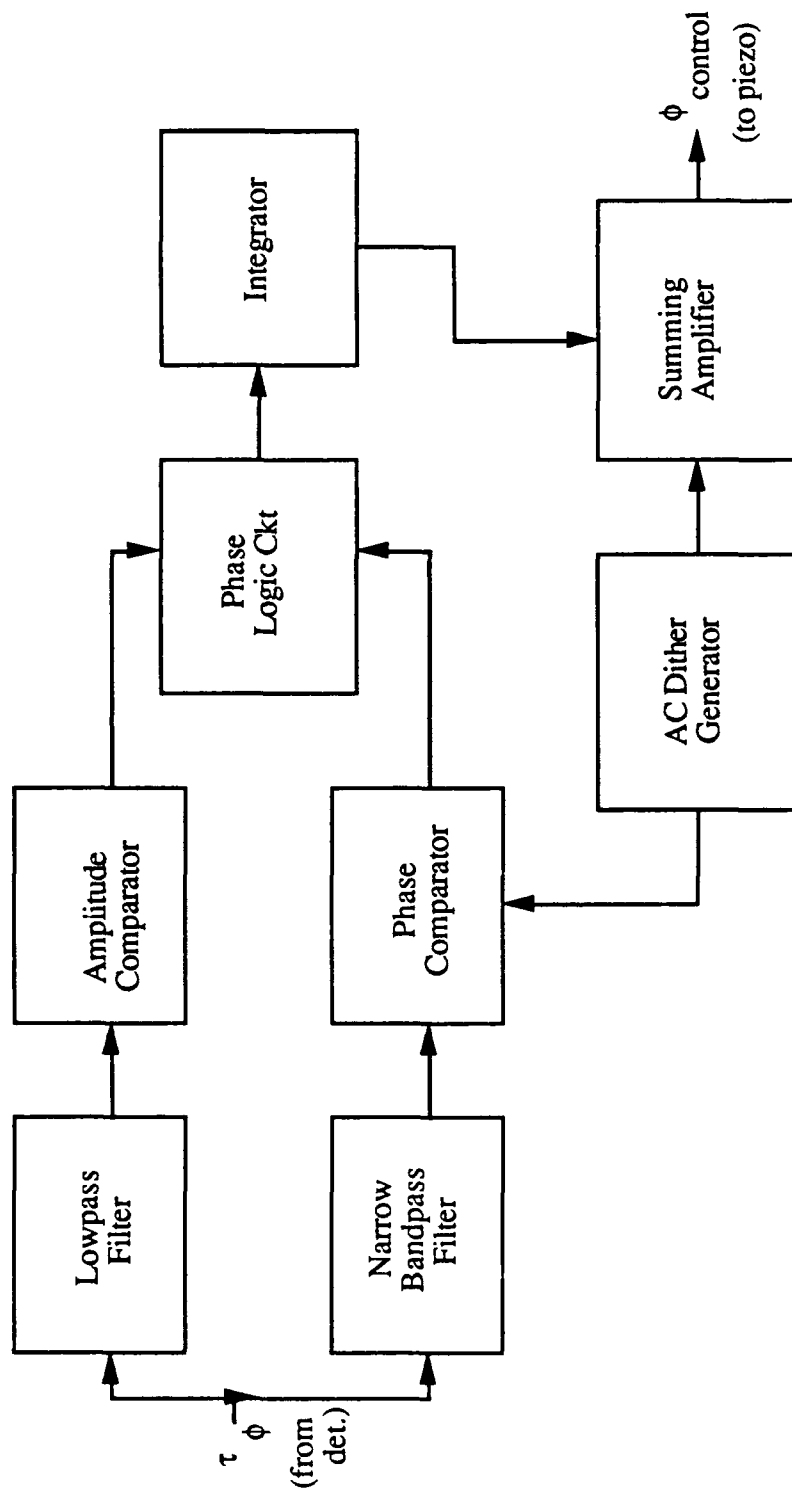
Fig. 21. Overview of Control Electronics System (φ–controller)
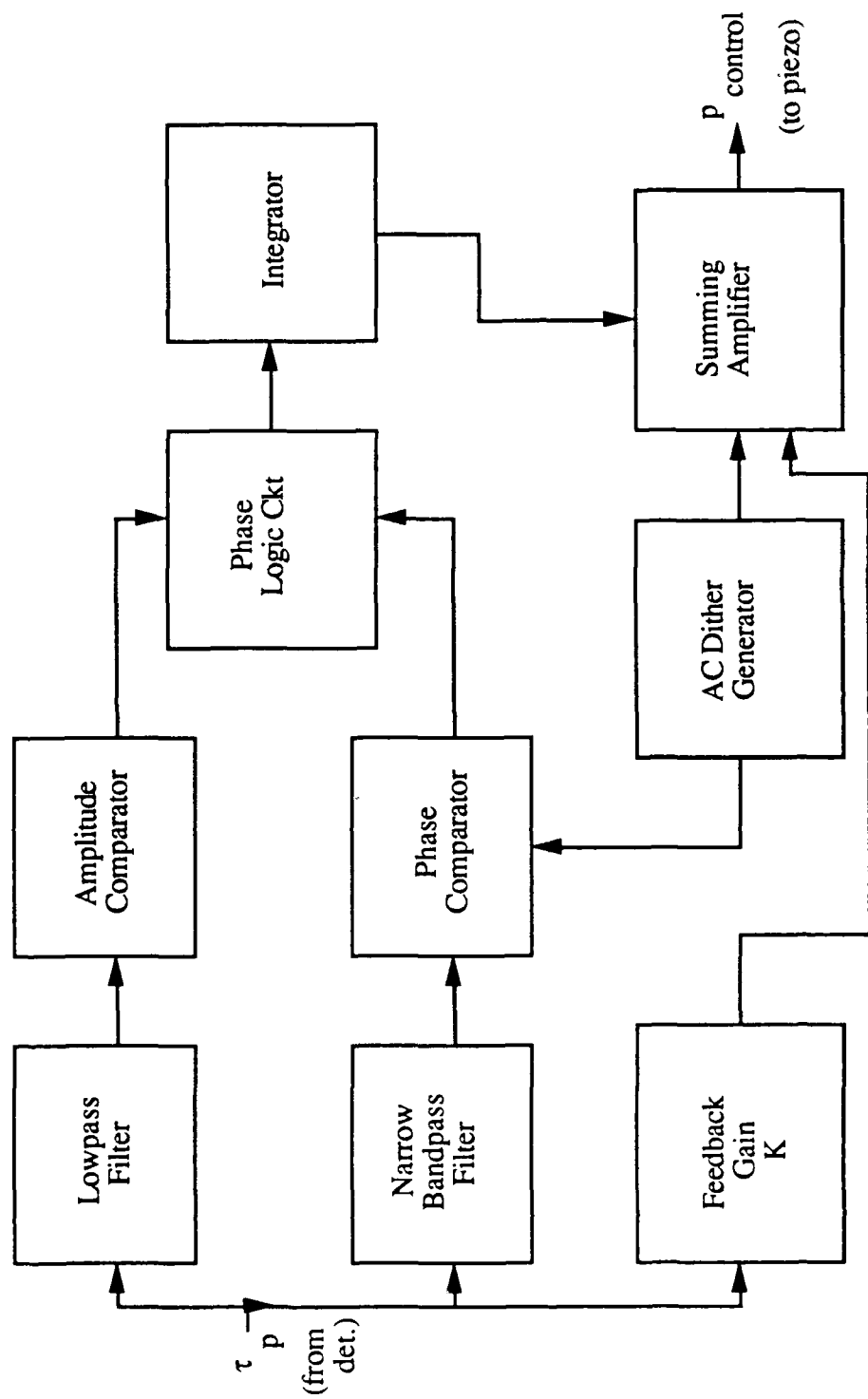
54

Fig. 22. Overview of Control Electronics System (P-controller)

Since the two sections of the controller operate similarly, only the P-controller's operation will be described, and any differences will be noted. The output transmittance from the interferometer is directed to the input filters, a low-pass and a narrow band-pass filter. The low-pass filter is a second order filter designed for a 3-dB cutoff at 1 KHz. It extracts the DC and low frequency (random temperature and pressure fluctuations) components from the transmittance and directs them to the bias level comparators located in the amplitude comparator block. In the bias level comparators, the voltage is compared to a preset voltage level required to maintain the proper operating point on the transmittance curve. Then the analog error voltage is converted to a digital control signal for the phase logic circuit. This control signal determines the direction of integration for the error signal integrator by selecting the voltage level (+5V or 0V) that is applied to the integrator.

The narrow band-pass filter removes the AC dither from the transmittance and directs it to a phase shifter. The dither enables the controller to select and maintain operation on the correct slope of the transmittance curve. The narrow band-pass filter is required to prevent other spurious signals from confusing the phase logic circuits. The bandpass of the filter is 1 Khz centered at 10.7 Khz (center frequency is arbitrary). An inherent delay in the dither generator is compensated for by a 90° phase shift circuit. When the dither is recovered by the filter, the phase shift circuit aligns it relative to the reference signal.

The dither is transformed to a square wave and compared to the reference signal in the phase comparator. The phase comparator determines if the dither received from the transmittance is in-phase or out-of-phase relative to the reference signal. The phase of the dither inverts about the common-mode compensation points of the output

transmittance (the extrema of the output from the compensating circuit). This inversion provides the additional information required to maintain the operating point on the correct slope of the transmittance curve. The output of the comparator determines which part of the phase logic circuit is enabled/inhibited. Earlier in Fig. 20, the phase inversions were shown.

The phase logic circuit, two 8-to-1 multiplexers, are selectively enabled or inhibited by the output of the phase comparator. The digital control signal from the bias level comparator picks one of eight preset input lines to supply a DC voltage (+5 V or 0 V) to the integrator. The integrator's output voltage will increase/decrease in response to the input voltage applied, thus providing a voltage to maintain the correct slope and proper bias level on the transmittance curve.

The output stage of the controller is the summing amplifier. It scales the control feedback, dither , and EOF (the ϕ-controller has no EOF) to the piezo. Through the summing amplifier, the integrator will maintain the bias control voltage on the phase shifter to lock the sensor output at its maximum sensitivity, common-mode compensated point. The integrator output, dither, and EOF are combined at the summing amplifier to produce this control signal.

The controller described above actively stabilizes the 1.5 MZI within its narrow region of maximum sensitivity and maintains the phase biasing necessary for CMC. It also provides a means for the sensor to initialize itself at start up. Since it uses a phase tracking method to maintain the proper phases, the controller is incremental and, thus, susceptible to a loss of information whenever the environmental noise exceeds the limits of its dynamic range. While this method of control does work, improvements to extend its dynamic range or an alternative approach should be investigated.

Chapter 6

Experimental Verification

The objectives of the experiment were to verify the feasibility of utilizing an active stabilization circuit to maintain the operation of an ES-CMC 1.5 MZI [33] over the narrow operating range required for common-mode compensation and high sensitivity and to quantify the minimum detectable measurand for this FOS. Previously it had been shown that the 1.5 MZI [34] exhibits a high sensitivity to small phase shifts superior to the 1.0 MZI. This was accomplished through adjustment of the feedback gain and initial phase biases. However, differential phase modulation caused by environmental perturbations created low frequency drifts that were indistinguishable from changes due to the measurand. This made it difficult, almost impossible, to perform accurate and repeatable minimum detectable phase measurement. Theoretically, it has been shown that a suitable means to minimize the effects of environmental disturbances (common-mode and random) and to achieve maximum sensitivity and linearity in the presence of differential phase modulation is achievable by incorporating a control scheme into the FOS. A description of the experimental setup and results follow.

6.1. Experimental Setup

A diagram of the experimental system is illustrated in Fig. 23. The system is comprised of a light source, an ES-CMC 1.5 MZI [35], three optical detectors and amplifiers, two division circuits, a controller circuit, and power supplies. Data
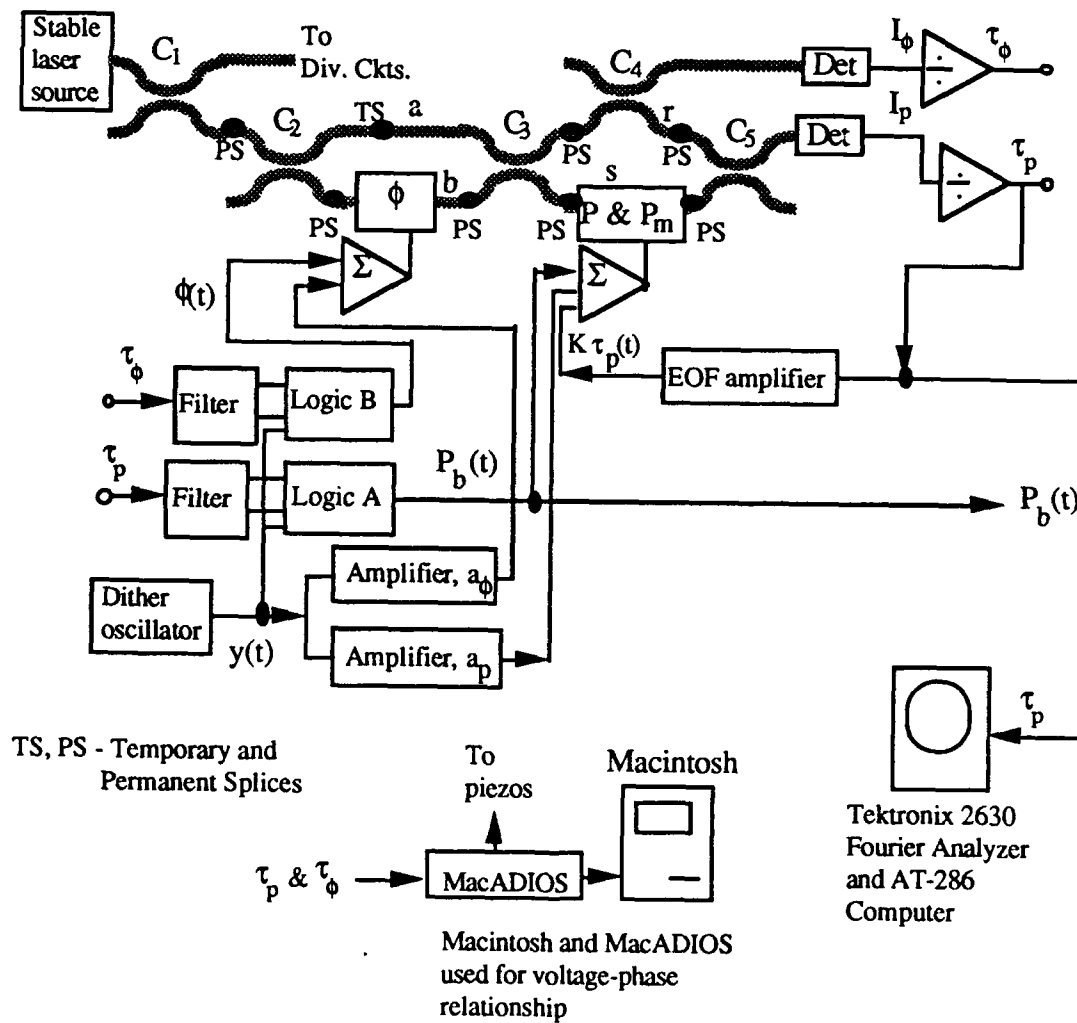
Fig. 23. Diagram of the Experimental System

acquisition and control is performed using a G. W. Instruments MacADIOS (Macintosh Analog/Digital Input/Output System) model 411 data acquisition system interfaced to an Apple Macintosh Plus computer and a Tektronix Personal Fourier Analyzer model 2630 interfaced to an AT 286 personal computer. An Interstate Electronics Corporation (IEC) FM/AM Function Generator model F-35 is used to simulate the measurand. The operation of the 1.5 MZI and the controller circuit has been detailed in earlier chapters and will not be repeated here except as needed to explain the data acquisition process.

A Uniphase model 106-1, 20 mW, Helium-Neon laser is the source of radiation. It is polarized and lases at $\lambda=0.6328$ μm. It has a single mode fiber pigtail and alignment mechanism for optimally coupling light directly into another fiber. The laser is spliced to a directional coupler and the directional coupler to the input fiber of the sensor using GTE lab (temporary) splices, part number W01140. These splices, as well as GTE elastomeric glass tube (permanent) splices, part number W01098, are used to connect separate components throughout the optical circuit. TS and PS in Fig. 23 denote temporary and permanent splices, respectively. The insertion loss for each type of splice is less than 0.2 dB. To insure minimum splice losses, a Newport F-BK2 optical fiber precision cleaving tool was used to cleave fiber end facets consistently. It produced end-faces perpendicular to better than 1° without fractures. The quality of the end facets were confirmed using a Newport F-IM1 Optical Microinterferometer.

The directional couplers used to insert and extract light from the sensor, C_1 and C_4, are Aster SMC-01-10-2-A-1-S fused biconical tapered directional couplers. They divide the output optical power ninety percent into one arm and ten percent into the other; thus, they are referred to as 90/10 couplers. Each coupler's insertion loss is less than 0.2 dB.

The 1.5 MZI optical configuration used in this experiment is built from low birefringence Newport F-SV single mode optical fiber and three Newport F-506B fused biconical tapered directional couplers. The fiber's index of refraction is 1.4606 [36], and the attenuation at λ=0.6328 μm is 10.54 dB/Km. The three directional couplers, C_2, C_3, and C_5, are 3-dB (50/50) power dividers. Each coupler has an insertion loss less than 0.8 dB. The optical path length difference was minimized to reduce the effects of temperature variations. The fiber path lengths are L_a = 300.8 cm, L_b = 300.9 cm, L_r = 380.0 cm, and L_s = 380.1 cm. These lengths are measured from directional coupler to directional coupler including the turns of fiber around the phase modulators. These small path length differences, 1 mm, represent a difference of approximately 1500 wavelengths, enough to allow passage of much of the common-mode noise. The interference circuit bounded by C_2 and C_3 is the compensating circuit, and the sensing circuit is bounded by C_3 and C_5. Temporary splices are used in the compensating circuit to facilitate direct experimental comparison between the 1.5 MZI and a 1.0 MZI.

Three phase modulators are located in the sensor. Each piezoelectric cylinder is of the PZT-5H variety. Two of them, ϕ and P, are 3.2 cm in outer diameter and have fifteen wraps of optical fiber tightly wound around them. The third cylinder, P_m, is 2.54 cm in outer diameter and has only one tightly wound wrap of optical fiber on it. PZT is a very efficient piezoelectric material. Therefore, in order to facilitate ease of measuring the voltage required for the minimum detectable measurand, P_m was chosen with smaller dimensions and wrapped with fewer turns of fiber. The fiber was secured to the modulators by a thin strip of cyanoacrylate (super glue) along the cylinders' lengths.

One significant deviation from 1.5 MZIs [37] previously reported is the elimination of the polarization controllers. It was discovered that for the short lengths (less than ten meters) involved for the 1.5 MZI, the polarization did not change drastically enough to warrant their incorporation. The low birefringence fiber used in the sensor's construction exhivits good polarization stability over distances of a few meters. If the polarization of the guided modes rotate in their respective arms prior to interfering, the fringe visibility will decrease and signal fading results; thus, the polarization controllers had been used in the earlier sensors to control fluctuations in the fringe visibility. Adjusting the polarization controllers proved very tedious and imprecise, because the sensor's output varies wildly each time the polarization controller is touched. A more significant effect on fringe visibility occurs from controlling the phase bias than adjusting the polarization.

The reference intensity from C_4 and the sensing and compensating circuit intensities from C_5 are detected using TRW OP593C phototransistors. It is here that the optical signal is converted to an electrical signal. The current from these phototransistors is converted to a voltage and amplified by the detector amplification circ iit shown in Fig. 24. These circuits were designed using Fairchild 741 operational amplifiers. The frequency response of the detector circuit is controlled by the feedback resistor in the current to voltage converter (first stage) of the amplification circuit. From the sheet of characteristic curves for the phototransistors, the highest frequency cutoff corresponds to a 10 KΩ feedback resistance. A 10 KΩ potentiometer was used as the feedback resistance for added flexibility. The second stage is required for inversion and amplification of the detected signal.
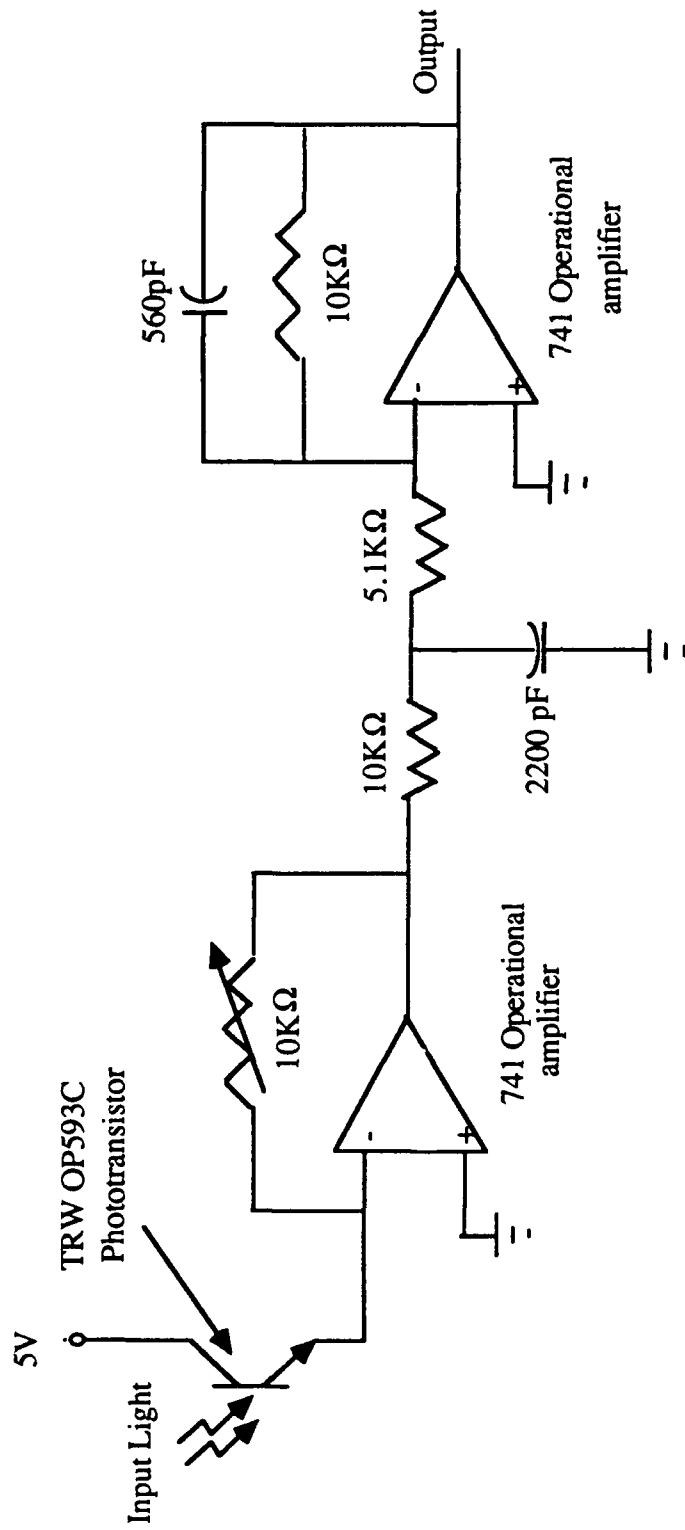
Fig. 24. Detector Amplification Circuit

Since intensity fluctuations from the optical source corrupts the sensor's ability to measure phase shifts, a method designed to reduce the intensity fluctuation effects is employed. The output intensities from the compensating and sensing circuits are divided by the reference intensity. The premise for this is any intensity fluctuations from the laser source appears in each of the three outputs, and dividing by the reference level normalizes the transmittances (output intensities divided by the input intensities), thereby diminishing the effects of intensity variations. The division circuit is an Analog Devices AD535JD internally trimmed integrated circuit divider. Fig. 25 shows the standard divider connection without external trimming resistors and its transfer function.

The output transmittances from the dividers are directed to the controller (described in Chapter 5), where the correct phase biases of the interferometers are maintained to simultaneously operate the sensor with common-mode compensation and high measurand sensitivity. The controller generates error signals and applies them to the phase modulators of the interference circuits as correction signals. BNC connectors on the front panel of the controller provide signals to the data acquisition systems. The MacADIOS determines the initial bias voltages and records the transmittance curves. The 2630 Analyzer records the time domain output and frequency spectrum of the sensor.

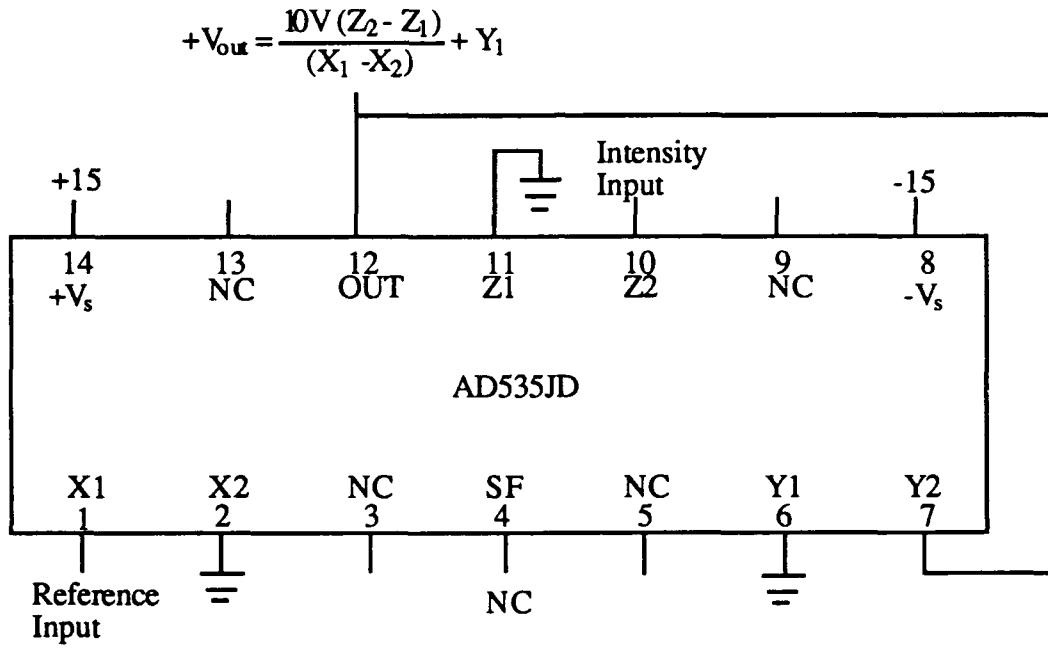$$+V_{out} = \frac{10V\,(Z_2 - Z_1)}{(X_1 - X_2)} + Y_1$$

Fig. 25. Division Circuit, AD535JD

6.2. Experimental Procedures and Results

Several experiments were done on the FOS system shown in Fig. 15 and described above. The objective of these experiments was to quantify the sensitivity of the 1.5 MZI. Data were collected for the sensor configured as a 1.0 MZI, a 1.5 MZI without EOF, and a 1.5 MZI with EOF. The 1.0 MZI, one of the most common configurations utilized in FOS construction, has had much reported on its performance; thus, it is used as the standard against which the 1.5 MZI's performance is measured. The design of the 1.5 MZI expedites quick conversion to a 1.0 MZI by removing one of the temporary splices in the compensating circuit of the 1.5 MZI. This insures that all parameters are equivalent for direct comparison between the 1.0 and 1.5 MZIs. In each of the configurations, the measurand is detected by the sensing circuit.

Until these experiments, the stability of the 1.5 MZI was not adequate to experimentally obtain a detailed minimum detectable phase (MDP) shift measurement with reliable repeatability. The performance of the 1.5 MZI was estimated from calculations of the maximum slope of the transmittance curve. The use of the Tektronix 2630 Fourier analyzer and the controller enabled these experiments to measure the minimum detectable measurand for each configuration and, as such, tested the feasibility of using a controller to stabilize the FOS in the presence of common-mode and random environmental noise. The controller had to control the phase drift in the optical circuit if the phase biases were to be maintained at specific values.

Since the principle feature of the 1.5 MZI is enhanced sensitivity and common-mode noise rejection, the sensor has to be biased in the region of maximum sensitivity and common-mode compensation. This is achieved by initializing and adjusting the

two phase biases appropriately. From computer simulations, the phase biases required for common-mode compensation were determined. Next, the voltage required on the phase modulators to achieve these phase biases was found experimentally. MacADIOS applied a linear voltage to the PZT (Lead Zirconate Titanate) cylinders and recorded the output transmittance. The record was then used to determine the voltage-phase relationships as illustrated in Fig. 26 and Fig. 27. The voltage corresponding to the desired phase is set into the controller by adjusting a potentiometer. The controller subsequently maintains the voltage level, thus the phase. A similar procedure is done for ϕ and P.

The first measurements taken scaled the output of the measurand phase modulator to convert between voltage and radians. In the sensing interferometer circuit, there are two phase modulators, one for the EOF and the other for the measurand. The two piezos are of different sizes, and the voltage-phase relationship for each is different. The voltage-phase relationship for the P phase modulator was obtained as described previously. However, since MacADIOS has an output voltage range limit of 20 volts (+10V to -10V) and the voltage needed to move the measurand piezo, P_m, through a 2π phase shift far exceeded 20 volts, the voltage-phase relationship for P_m cannot be determined directly. Instead, it was obtained through a relative measurement with P.

A sine wave of three millivolt peak-to-peak (p-p) amplitude was applied to the P piezo, and the output, shown in Fig. 28, was recorded using the Fourier analyzer. This voltage caused a measurand signal which peaked at -39 dB to appear in the frequency spectrum. Then, the voltage was transferred to the P_m phase modulator and increased until a similar pulse of -39 dB appeared in its frequency spectrum. Fig. 29 is
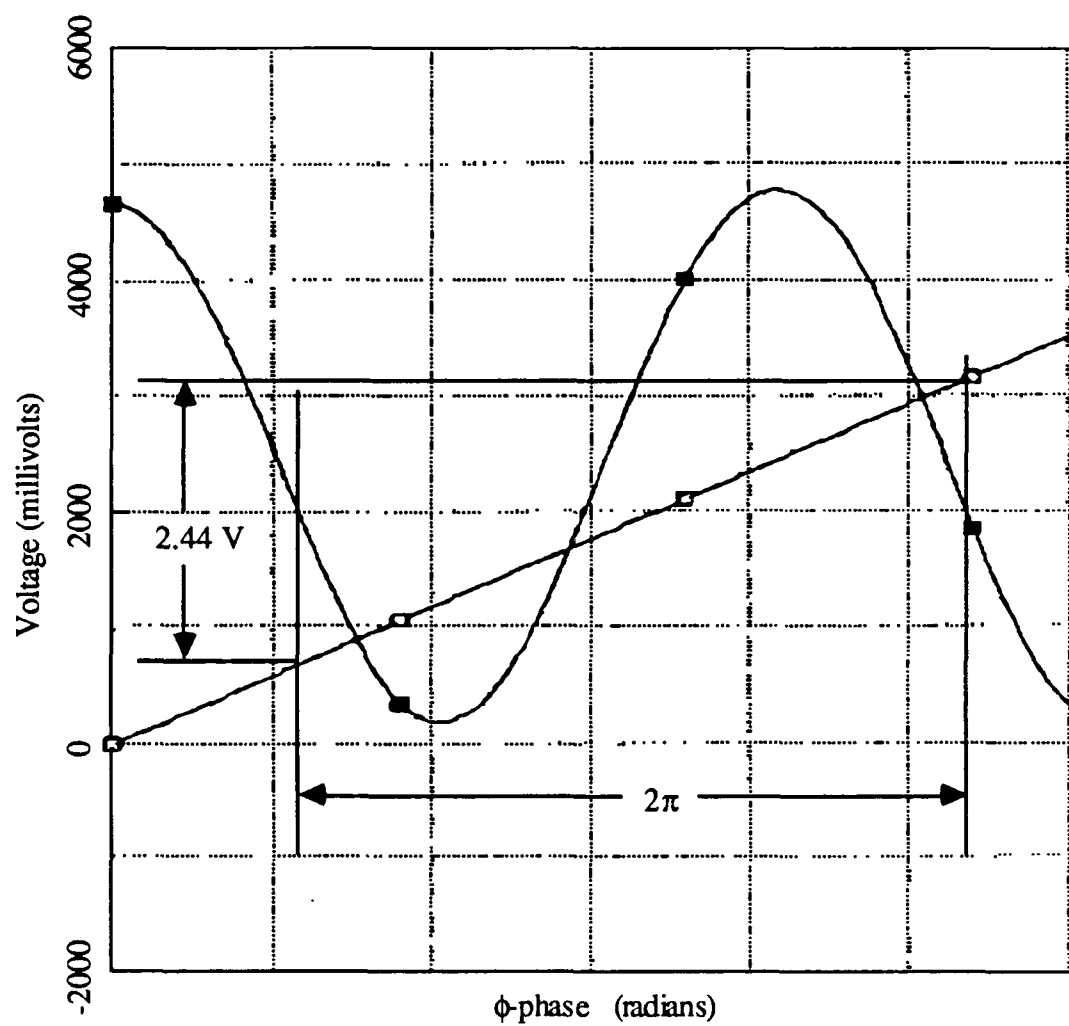
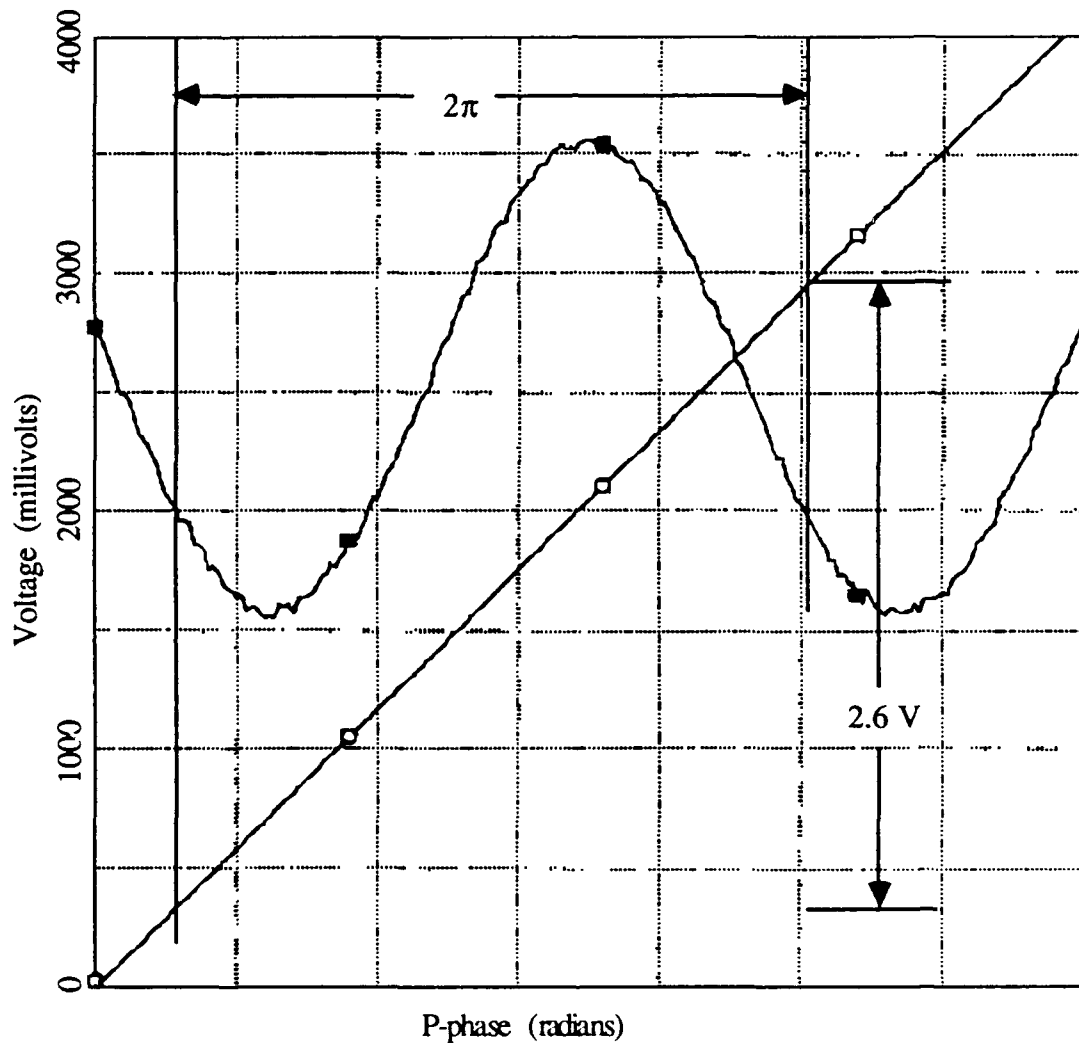Fig. 26. The Compensating Circuit Phase Bias vs. Voltage

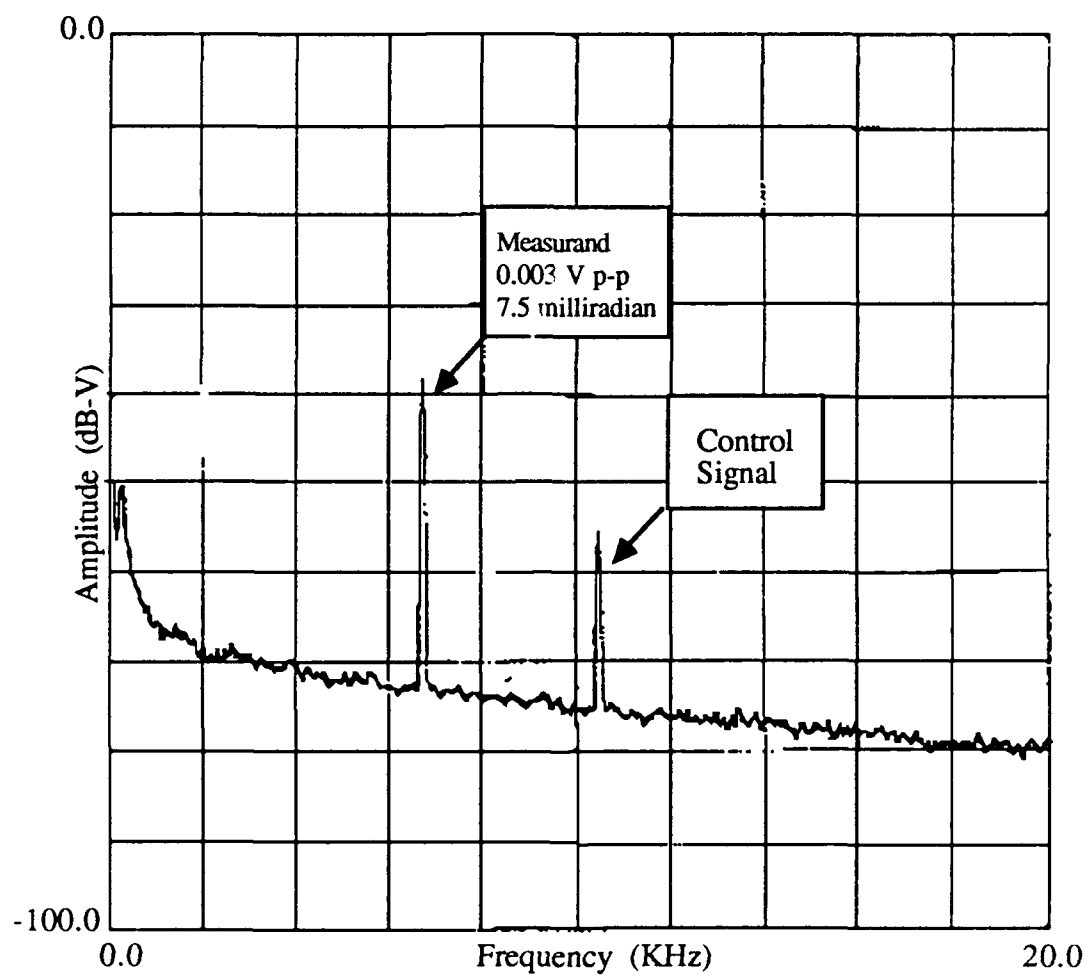Fig. 27. The Sensing Circuit Phase Bias vs. Voltage

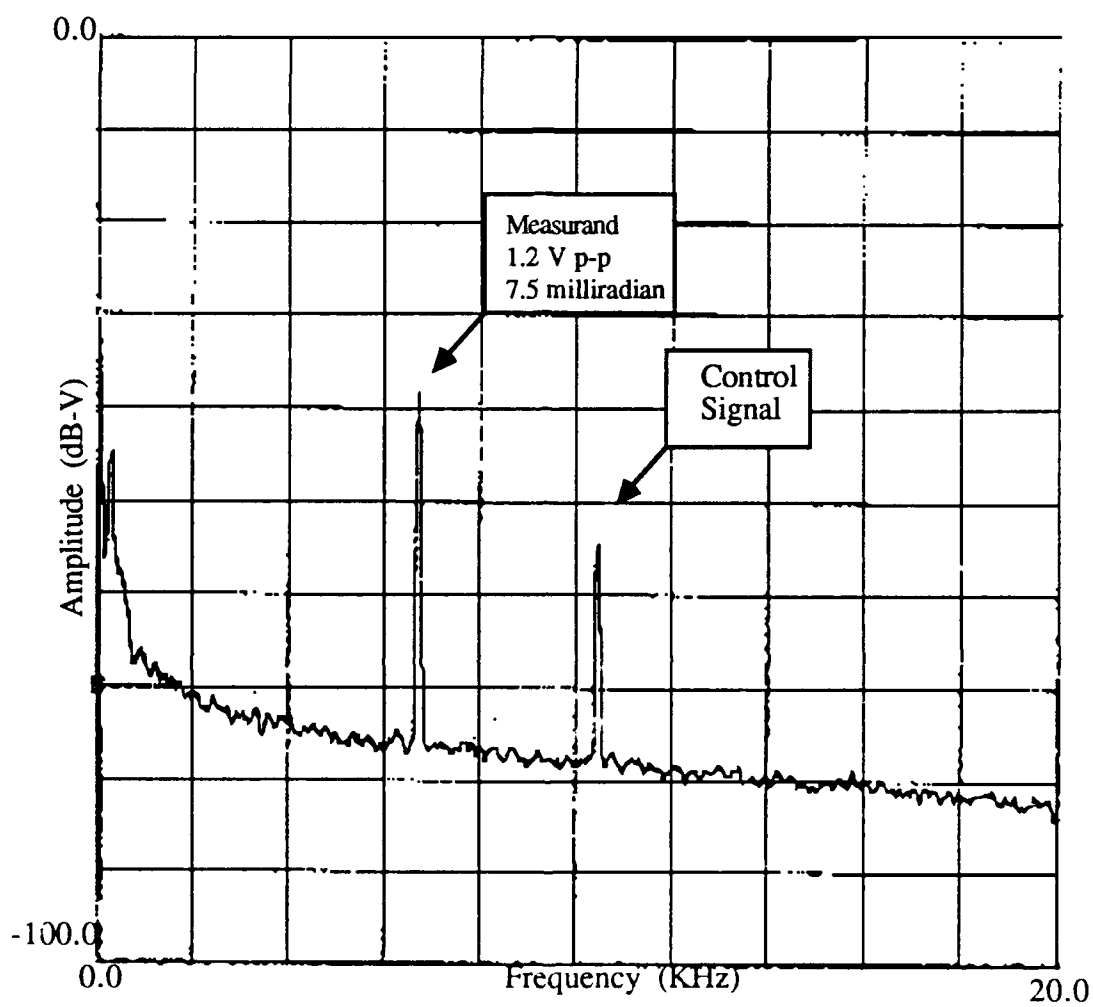Fig. 28. Relative dB Measurement for P Phase modulator

Fig. 29. Relative dB Measurement for P_m Phase Modulator

a record of P_m's frequency spectrum. At this voltage level, the phase shift imposed on P_m is equivalent to the phase shift imposed upon P by the three millivolt signal. The sinusoid being applied to P_m was measured as 1.2 volts p-p. From the voltage-phase relationship of P (Fig. 27), it is calculated that a three millivolt change corresponds to 7.5 milliradian phase shift; therefore, the phase shift imposed on P_m by the 1.2 volts p-p sinusoid was also 7.5 milliradian. Now, the phase shift due to any voltage on P_m can be calculated from the applied voltage using the linearity of the voltage-phase relationship and the relative measurements of the P and P_m phase modulators.

Removing one of the temporary splices in the compensating circuit, the FOS is reconfigured as a conventional Mach-Zehnder sensor (1.0 MZI). The second measurements are undertaken to establish the baseline sensitivity in a 1.0 MZI for comparison to the 1.5 MZI. The 1.0 MZI is biased for maximum sensitivity at its quadrature point, $P = \frac{\pi}{2}$. While observing the Fourier analyzer, the voltage applied to P_m is reduced until the associated pulse in the frequency spectrum is no longer discernible above the noise floor (signal to noise ratio of unity). Then, the voltage is increased until the pulse is just barely visible above the noise floor. At this point the voltage is measured as the MDP shift.

The MDP of the 1.0 MZI, illustrated in Fig. 30, was measured with a ten millivolt p-p sinusoid being applied to P_m. An enlarged view, displayed in Fig. 31 and accomplished through a zoom-in feature of the Fourier analyzer, more clearly displays the measurand signal above the noise. The voltage utilized corresponds to a phase shift of 62.5 μ radian/$\sqrt{Hz}$, approximately an order of magnitude worse than the state-of-the-art 5 μ radian/$\sqrt{Hz}$ [38]. (Note: The phase shift is described in units of μ radian/$\sqrt{Hz}$ as this provides a normalized measure, spectral density, where spectra can
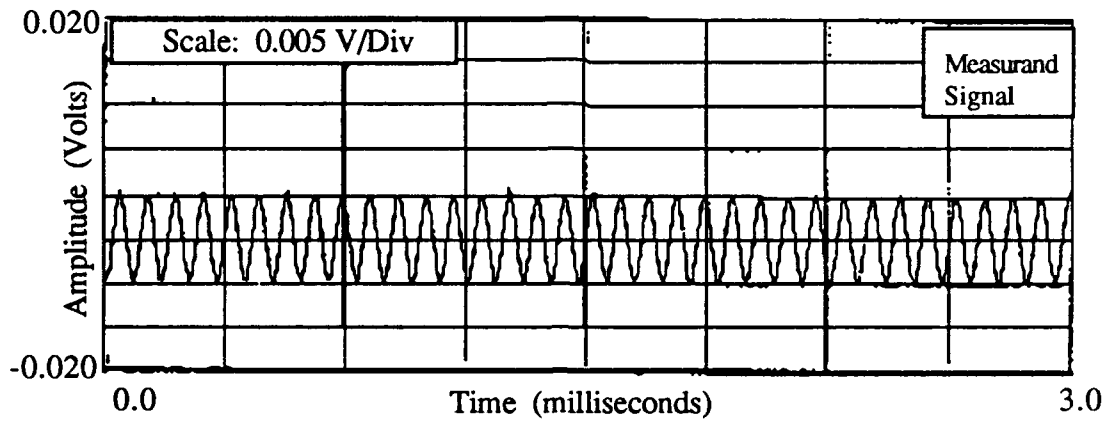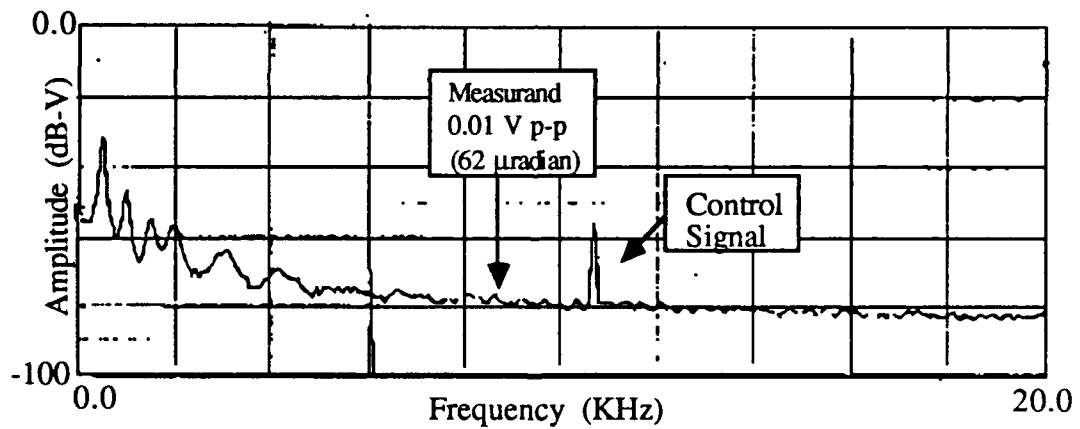
Fig. 30. MDP Shift of the 1.0 MZI. a.) Time domain signal applied as the measurand. b.) Minimum detectable phase shift measured in the frequency domain.
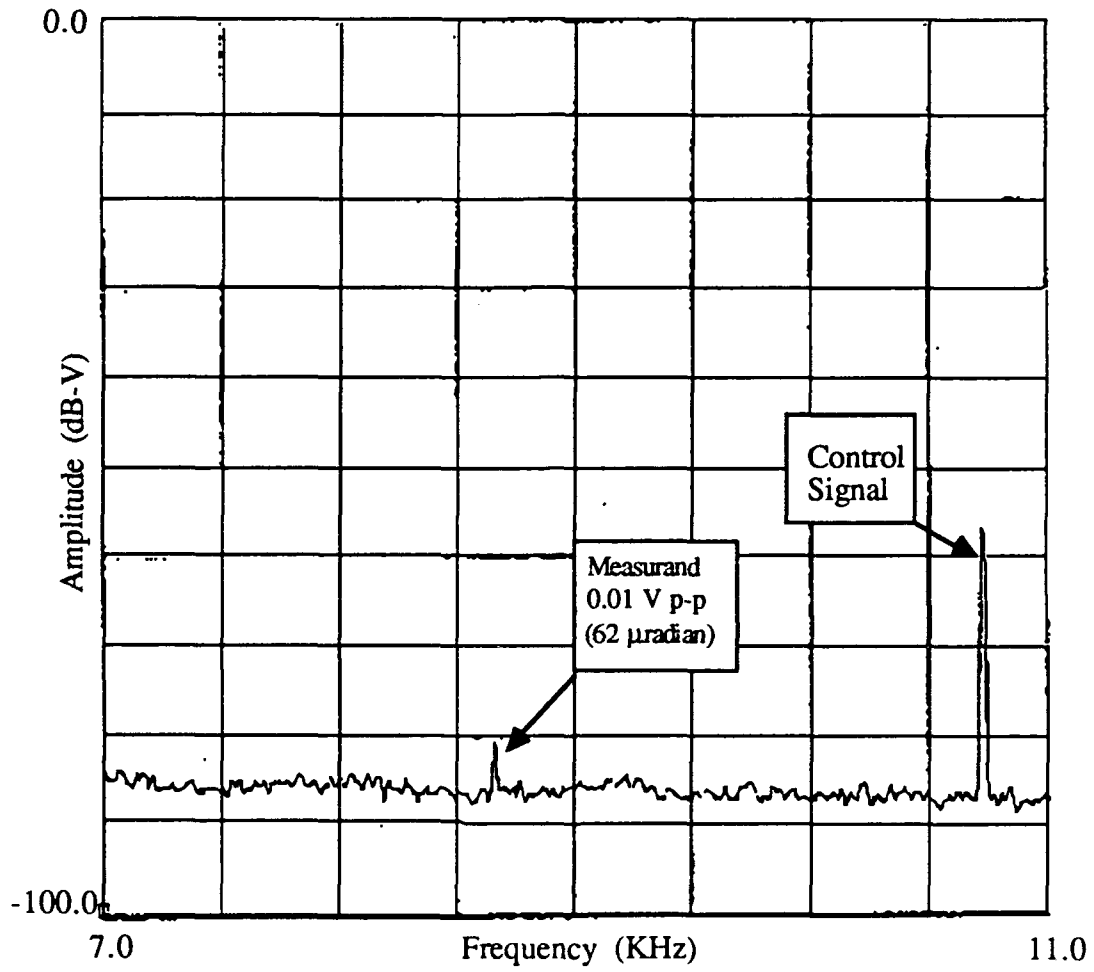
Fig. 31. Enlarged View of MDP Shift of the 1.0 MZI

be compared directly since the measurements are given for the same bandwidth.) This difference between the measured phase shift and the state-of-the-art value is attributable, in part, to the conservative measurement of the experimenter. The MDP was determined using the broadband spectrum rather than the enlarged view which would have allowed further reduction of the measurand voltage. Also, the noise generated in the controller electronics and from the background environment contributed to an increased noise floor. A drawback of the conventional Mach-Zehnder is its inability to reduce its sensitivity to environmental perturbations without some elaborate method of signal processing or complicated circuitry. Little effort was expended to completely isolate the sensor from the environment. While the FOS was enclosed in a polyvinyl (PVC) container to impede direct air currents from the sensor, the majority of tests were conducted under conditions designed to minimally control the environment.

The sensitivity of the 1.5 MZI with and without EOF was the third measurement recorded. The open path in the compensating circuit was closed by replacing the temporary splice, configuring the FOS as a 1.5 MZI. Since a myriad of phase biases satisfy the condition for common-mode compensation and high sensitivity, two bias values were chosen arbitrarily. The bias points were constrained to maximize the measurand sensitivity at an environmental sensitivity minima. The controller was adjusted to maintain the interference circuits at $\phi = \frac{5\pi}{4}$ and $P = \frac{3\pi}{4}$. The procedure to perform the MDP measurement was identical to that done on the 1.0 MZI above. The minimum phase shift measured eight millivolt p-p or 50 μ radian/$\sqrt{\text{Hz}}$. Without changing any other parameters, EOF was added to the sensor, and the amplitude of the frequency spectrum pulse increased approximately 55 dB (562 times).
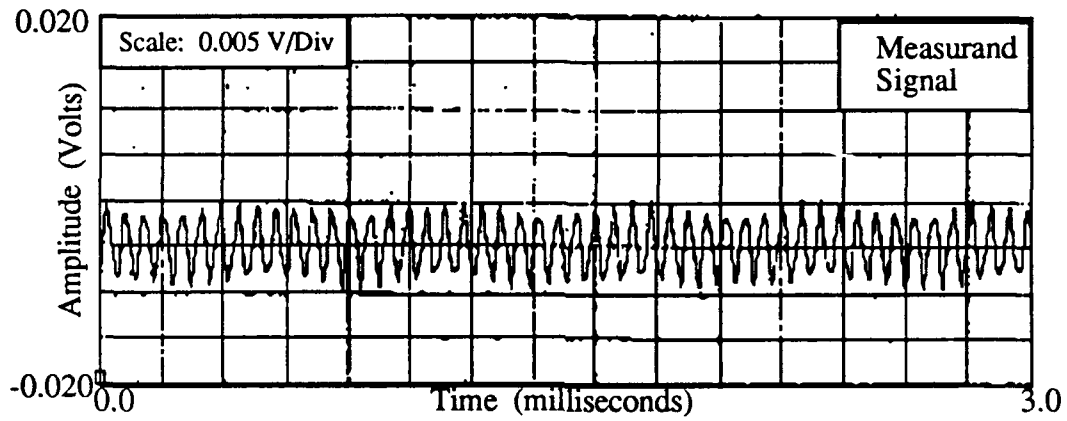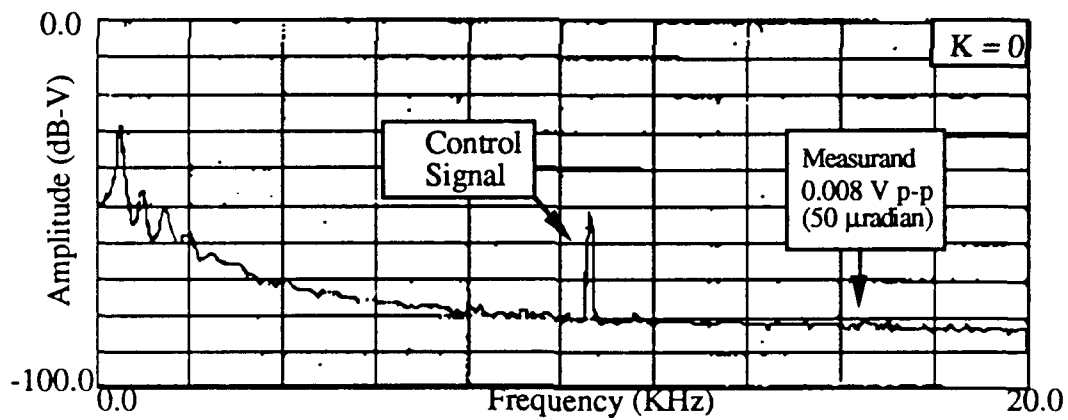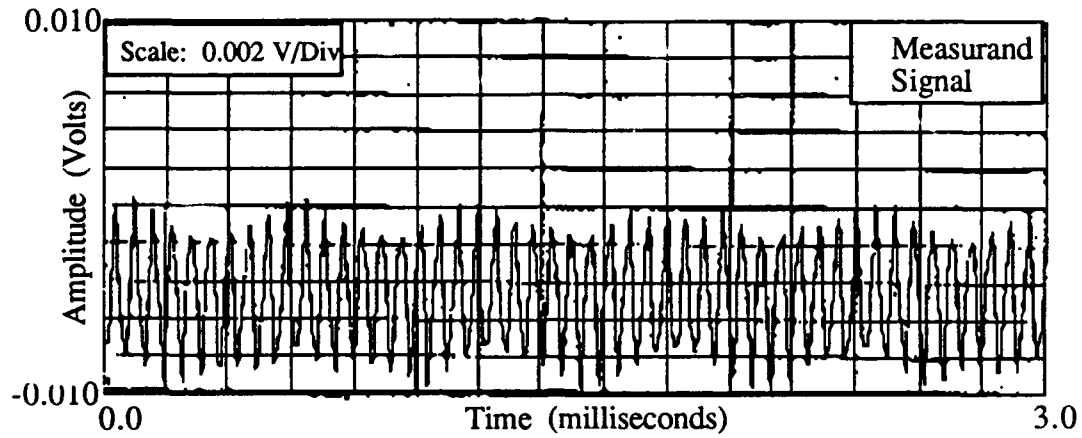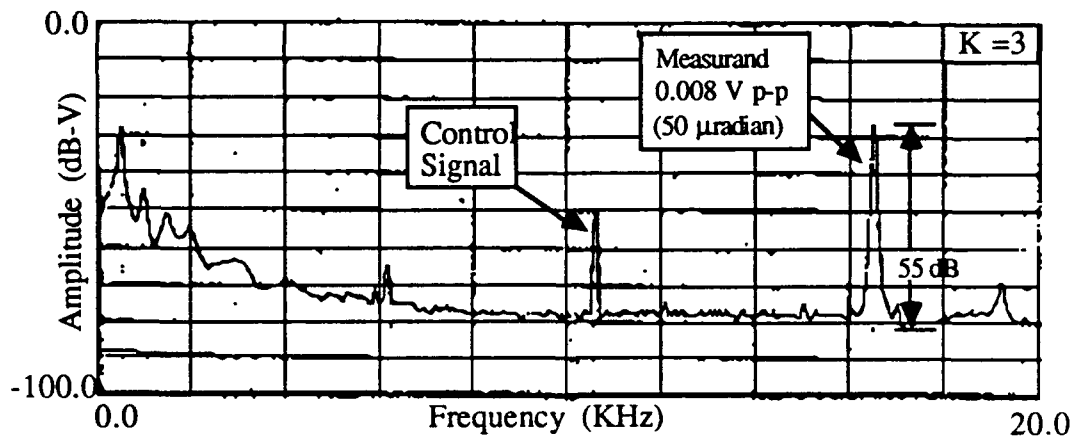
Fig. 32. MDP Shift of the 1.5 MZI without EOF, δP_m = 8 millivolt p-p
a.) Time domain signal applied as the measurand. b.) Minimum
detectable phase shift measured in the frequency domain.

Fig. 33. MDP Shift of the 1.5 MZI with EOF, $\delta P_m = 8$ millivolt p-p
a.) Time domain signal applied as the measurand. b.) Minimum
detectable phase shift measured in the frequency domain

A MDP of 89 nanoradian/√Hz (≈0.09 μ radian/√Hz) was recorded. Figures 32 and 33 show the power spectral output of the FOS without and with EOF. In order to verify the enhanced sensitivity, a second measurement was taken. This measurement used a measurand signal of 40 millivolt p-p (250 μ radian phase shift). When EOF was added, the measurand signal increased approximately 55 dB again. This indicated a MDP shift of 400 nanoradian/√Hz (0.4 μ radian/√Hz), an order of magnitude lower than the reported state-of-the-art. The spectral output for these measurements are displayed in Figs. 34 and 35.

Common-mode compensation was investigated during the fourth battery of tests. Wavelength drift of the source, intentionally enhanced by sweeping the source frequency, normally provides a simple means to demonstrate common-mode effects. Since the laser used in this experiment had no such feature for sweeping its frequency, long term data collection was used instead. The data were taken when the laser was first turned on as this most likely provided the least stable laser output. Thermal shock and mechanical vibration to the laser were used to create a wavelength drift. No conclusive evidence of common-mode effects were observed. This is likely attributable to a stable laser output and the more dominant effects from random noise overshadowing the common-mode effects.

A comparison of the controlled and free running spectral responses for the 1.5 MZI confirms that the noise floor for the FOS is limited by the electronic noise from the controller. The noise results from poorly shielded, wire-wrapped electronics. The noise floor is shown to be approximately ten decibels lower when the interferometer is uncontrolled (Fig. 36) than when the controller is allowed to stabilize the sensor. A more careful design of the control system electronics should lower the noise floor.
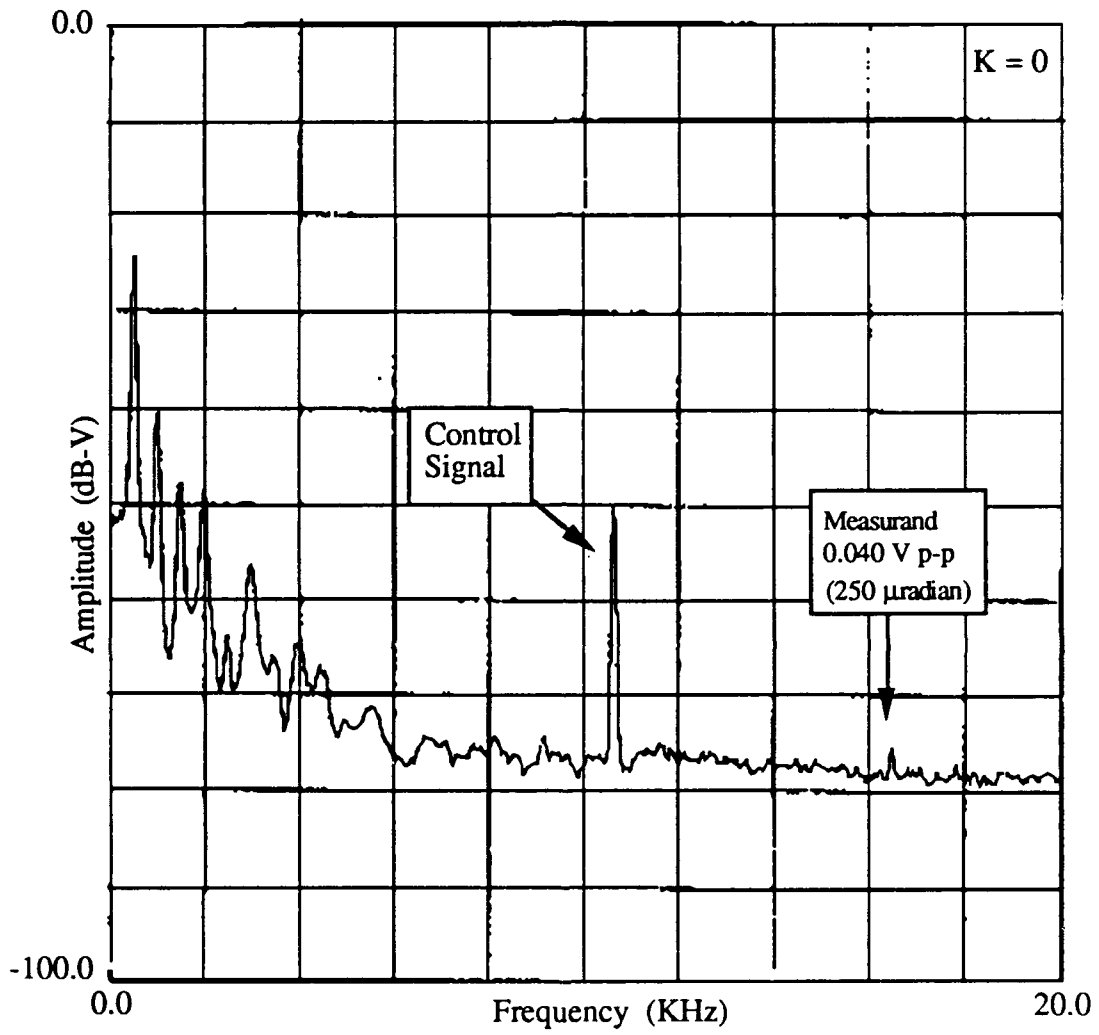
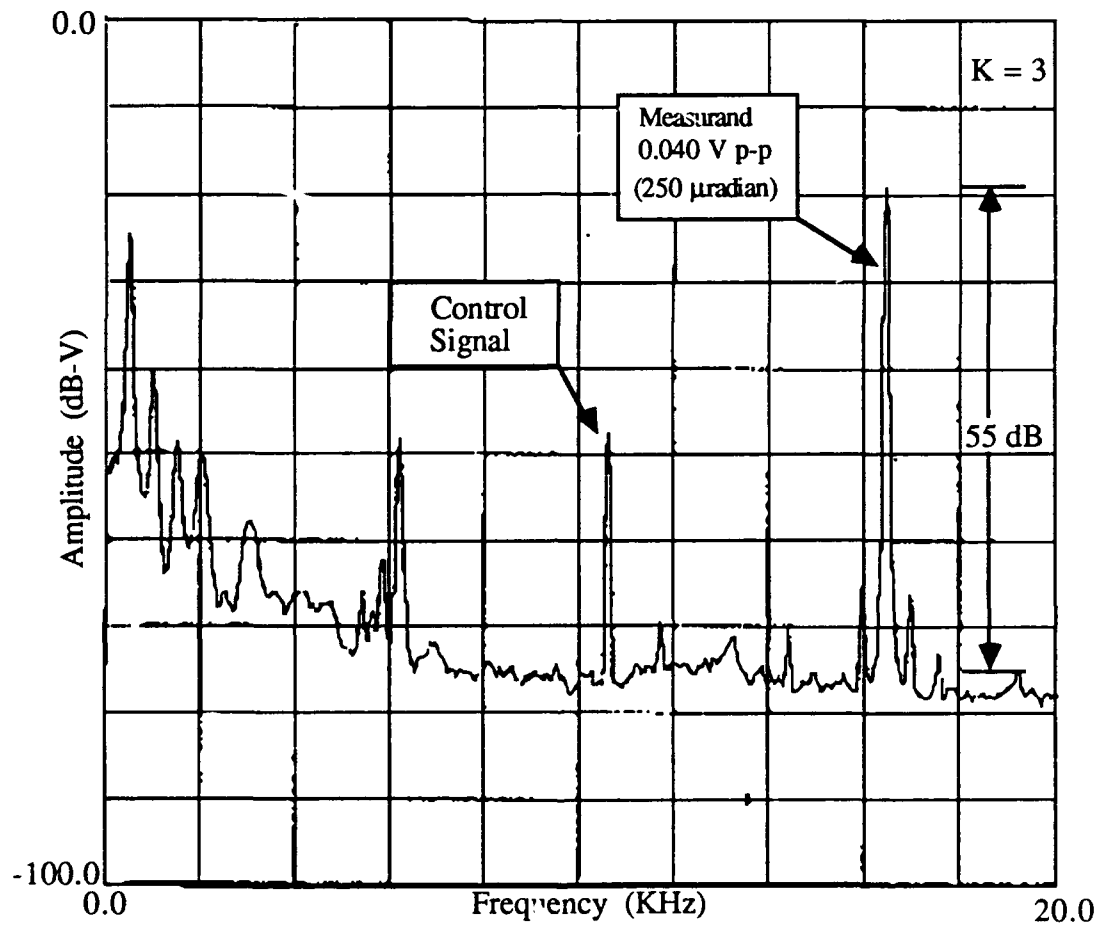Fig. 34. MDP Shift of the 1.5 MZI without EOF, δP_m = 40 millivolt p-p

Fig. 35. MDP Shift of the 1.5 MZI with EOF, $\delta P_m = 40$ millivolt p-p
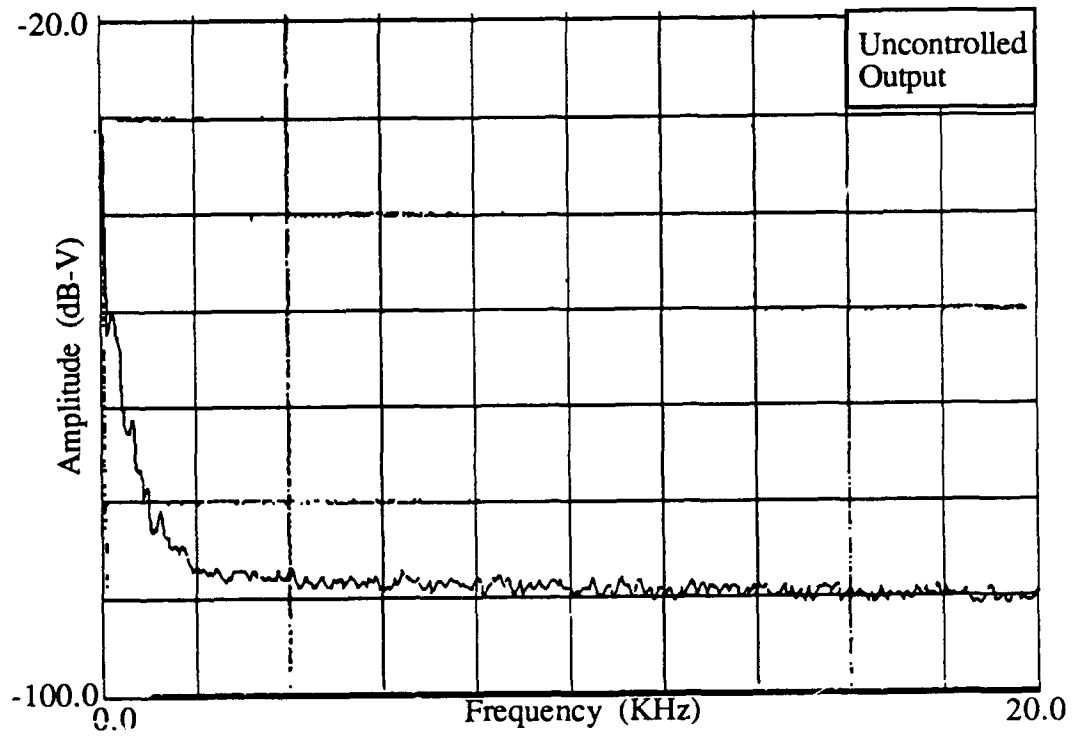
Fig. 36. Noise Floor of the 1.5 MZI

These experiments have shown that active stabilization of the 1.5 MZI is possible. The controller maintained the optical phase biases accurately enough that the 1.5 MZI could achieve CMC in a region of high sensitivity. The experimental results, in general, confirmed the theoretical predictions and successfully quantified the performance of the 1.5 MZI. Further, they have proven that when the feedback gain and initial phase biases of the 1.5 MZI is controlled, the performance of the 1.5 MZI exceeds that of the conventional Mach-Zehnder optical circuits.

Chapter 7

Conclusion

The purpose of the research reported in this dissertation was to describe the design and construction of an active stabilization controller and its interface with an interferometric FOS--the ES-CMC 1.5 MZI [41]. The feasibility of employing this active stabilization circuit to maintain the operation of an ES-CMC 1.5 MZI over the narrow operating range required for common-mode compensation and high sensitivity was demonstrated. Thus, a suitable means to minimize, even eliminate, the effects of environmental disturbances (common-mode and random) and to achieve maximum sensitivity and linearity in the presence of differential phase modulation was proven. This research shows that the incorporation of a control scheme into the FOS can improve the ability of the sensor to measure minute phase shifts employing EOF over two orders of magnitude (100 times) more than without EOF. More importantly, the FOS exhibited nearly a full order of magnitude (10 times) improvement in sensitivity beyond the state-of-the-art performance reported to date [42] for the conventional Mach-Zehnder optical circuit. The experimental result achieved using the phase tracking approach to signal processing was a minimum detectable phase shift of 0.09 μ radian/$\sqrt{}$(Hz).

This result is even more impressive when considered in light of the fact that the control system was implemented with wirewrapped electronics and standard (not extremely low noise) electronic components. Also, no extraordinary effort beyond isolating the body of the sensor from direct air currents and using standard grounding

procedures for the electronics was made to minimize the environmental or electronic noise.

The relationship between the phase biases and the electro-optic feedback gain of the 1.5 MZI was balanced to minimize common-mode noise effects and maximize the sensor's sensitivity. A correction signal was generated within the controller and applied to the phase shifters in each interference circuit whenever a difference between the preselected and actual operating points was detected. Thus, the controller maintained the phase biases of each interference circuit at a prescribed optical phase value chosen for CMC. The EOF gain was set for the maximum sensitivity achievable just prior to reaching optical bistability. The gain was adjusted by varying the input resistance of the output summing amplifier until the desired gain was reached.

While experimental investigations carried out on the FOS did not conclusively verify the computer simulations illustrating the effects of common-mode compensation, they did corroborate the theoretical predictions and simulations for the effects of electro-optic feedback on the sensor's transmittance curves. The apparent reason common-mode compensation was not conclusively substantiated was that the common-mode contribution to the total noise in this circuit was very small; thus, any changes resulting from common-mode compensation were overshadowed and could not be observed. As the noise floor of the electronics controlling the FOS is reduced, the common-mode contribution to the total noise will become dominant, and common-mode compensation will become more apparent.

Future research should be directed towards the investigation of alternative signal processing techniques. While phase tracking provides a means to initialize the system at startup and to maintain the FOS's operation in the region of high sensitivity, it

requires relatively large piezoelectric phase modulators to do so. Size might constrain the use of these modulators in multielement sensors. Also, the use of phase modulators preclude remote operations since electronics are necessary in the interferometer for stabilization. The phase tracking method is incremental and must utilize fast reset circuitry to reset itself whenever the environmental noise exceeds the limits of its dynamic range. Resetting itself causes loss of information and adds additional noise. Alternative approaches might include heterodyning, dual wavelength, and wavelength dithering.

Refinements of the phase tracking method should include improvements in the frequency response, stability, and dynamic range. The frequency response is limited by how fast the piezoelectric phase modulators can respond to mechanical deformations. Since the EOF gain is applied to a piezoelectric phase modulator in the P-loop and the frequency response of this feedback loop must be greater than any measurand variations sensed, the ability of the phase modulator to track the changes imposed on it ultimately establishes the upper frequency limit for the sensor. The use of alternative phase modulators should be investigated. Improvements to the stability of the controller through faster electronics should be studied, because faster electronics would mean that the phase biases and EOF gain could be more precisely controlled. Thus, the FOS could operate with even greater sensitivity before the onset of optical bistability. Finally, techniques that could extend the dynamic range of the FOS should be sought as this would allow the sensor to be utilized over a much broader range of applications. The same sensor could measure with accuracy displacements from decimeters to fractions of picometers.

Though the 1.5 Mach-Zehnder is not fully developed, it has demonstrated its potential to measure extremely small displacements. This makes it a candidate for replacing conventional sensors in a variety of applications. Hopefully, the research reported in this dissertation will contribute to the commercial appearance of the 1.5 Mach-Zehnder in measuring instruments and controls where its attributes can be fully exploited.

Appendix A
List of Terms

dB--decibels

DC--Direct Current

EOF--Electro-optic Feedback

ES-CMC--Enhanced Sensitivity, Common-mode Compensation

FOS--Fiber Optic Sensor

KHz--Kilohertz

LED--Light Emitting Diode

MDP--Minimum Detectable Phase

MZI--Mach-Zehnder Interferometer

PZT--Lead Zirconate Titanate

V--Volt

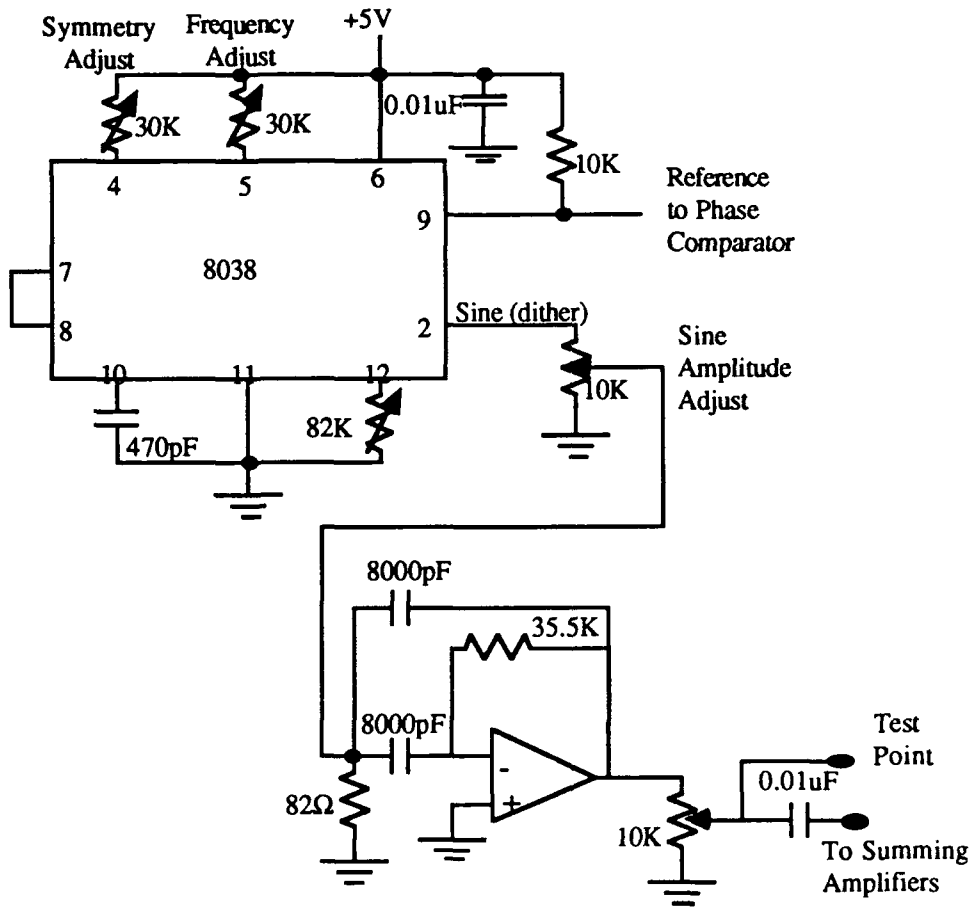# Appendix B
Schematics of the Controller

Fig. B-1. The Dither and Reference Generator

Dither and reference generator--The dither and reference generator is an ICL 8038 Precision Waveform Generator/Voltage Controlled Oscillator. It produces sine, square, triangular, sawtooth, and pulse waveforms with high accuracy. The

operating frequency can be selected from 0.001 Hz to 300 KHz. The square waveform is applied to the phase comparator circuits of each section as the reference signal. The sine waveform is transmitted to the ϕ- and p- piezos via the summing amplifiers as the dither. Because of the method used for signal generation within the monolithic device, there is an inherent phase shift of 90° between the square and sine waveforms. A narrow band filter is employed to remove any harmonics from the sinewave and to insure that the sinewave is undistorted.
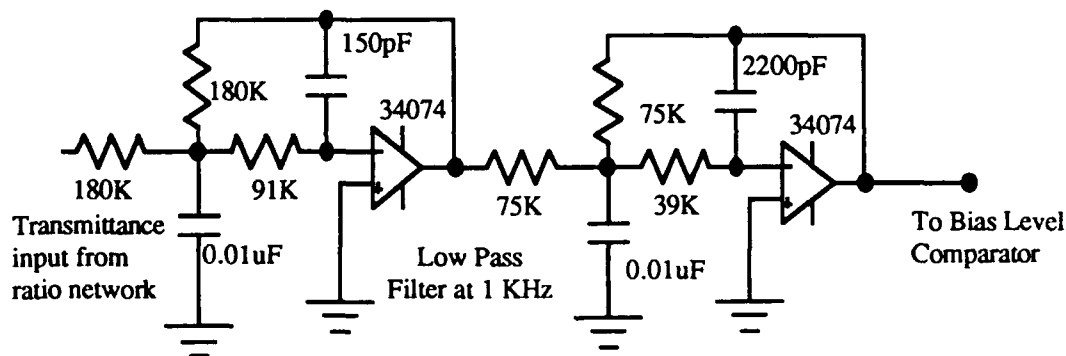

Fig. B-2. The Low-pass filter

Lowpass filter--The low-pass filter is a second order filter designed using a Motorola MC-34074AP Operational Amplifier. The 3-dB cutoff is at 1.0 KHz. The filter extracts the DC and low frequency components from the transmittance signal. This DC bias and environmental fluctuation voltage is filtered to maintain a relatively constant FOS transmittance output.
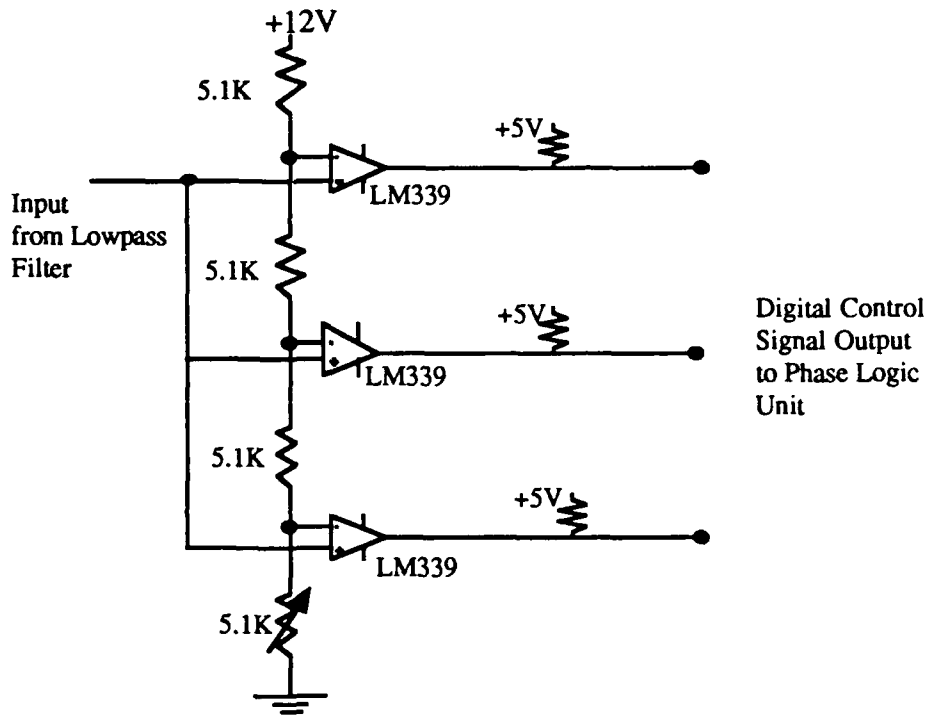
Fig. B-3. The Bias Level Comparators

Bias level comparators--The comparators are National Semiconductor Corp. LM-339 comparators arranged to convert the analog bias voltage from the low-pass filter to a digital control signal for the phase logic circuit. The analog bias voltage is compared to a preset voltage level required to maintain the proper operating point on the transmittance curve.
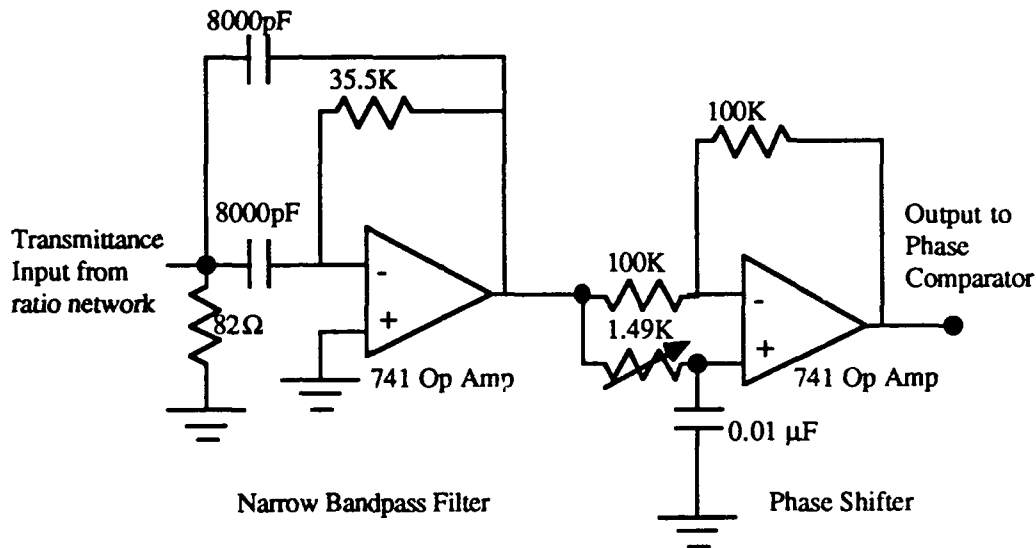
Fig. B-4. The Narrow Band-pass Filter and Phase Shifter

Narrow Bandpass filter and phase shifter--The narrow bandpass filter and phase shifter are designed from a Motorola MC-34074AP Operational Amplifier. The filter is a Butterworth design with a bandpass of 1 KHz centered at 10.7 KHz. The 90° phase shifter compensates for an inherent delay in the dither and reference generator.
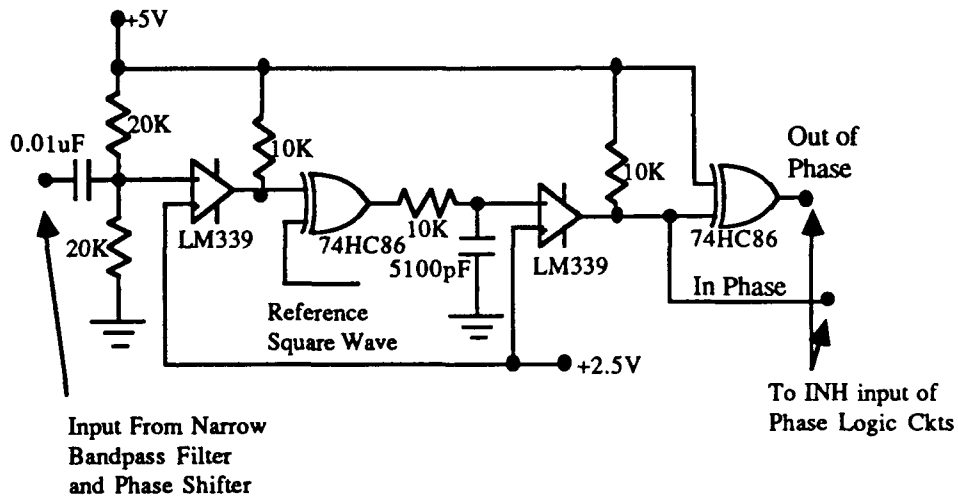
Fig. B-5. The Phase Comparator

Phase comparator--The phase comparator consists of two MM-74C86N exclusive-or (EX-OR) gates and two National Semiconductor Corp. LM-339 comparators. The dither (a sinusoidal signal) is converted to a square wave by the first comparator. The relative phase of the square wave and the reference signal results in a digital enable/inhibit signal being generated by the EX-OR/comparator network.
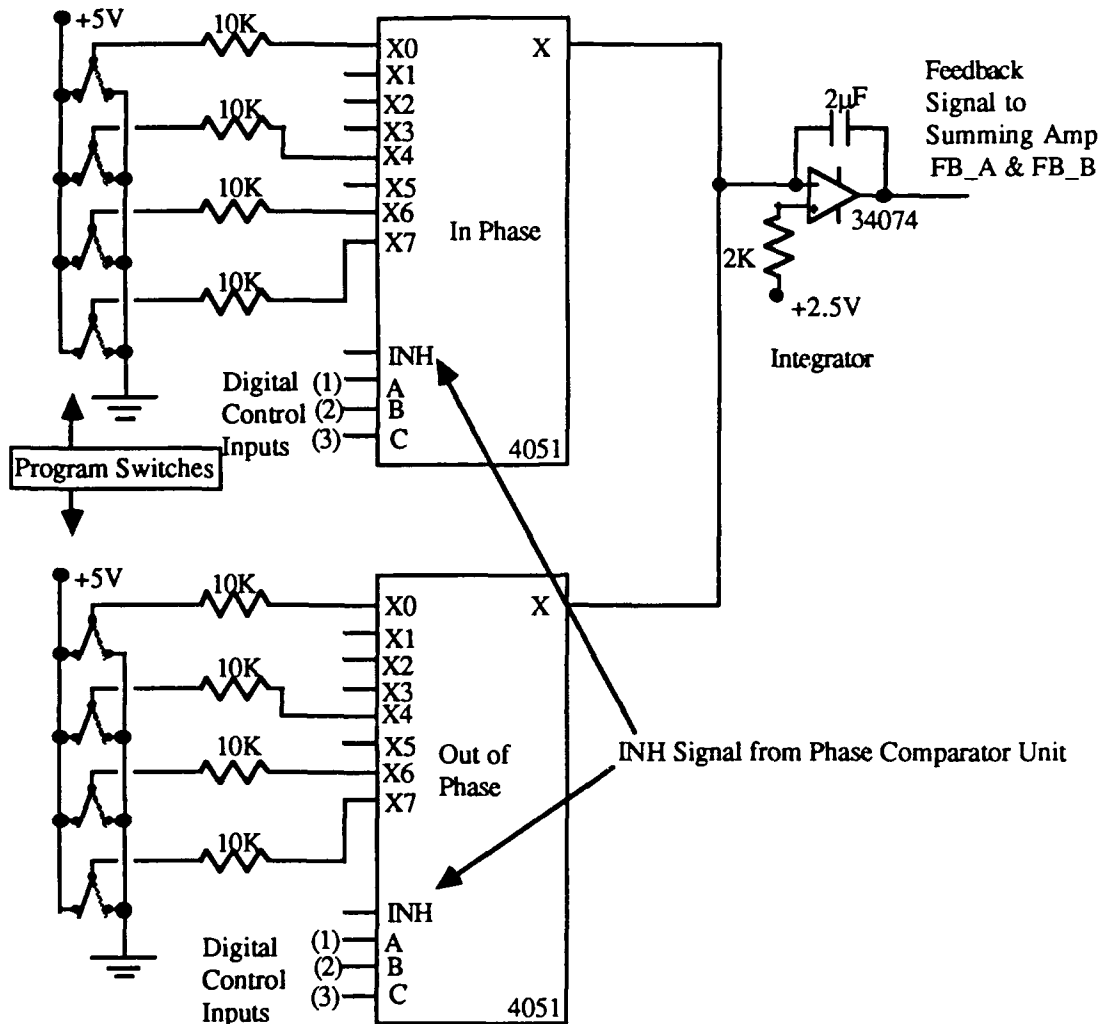
Fig. B-6. The Phase Logic and Integrator Circuits

Phase logic and integrator circuits--This circuit comprises two RCA CD-74HC4051E 8-to-1 multiplexers that provide a DC voltage (+5V or 0V) to the integrator to maintain the correct slope and proper bias level. The digital control signal from the bias level comparator picks one of eight preset input lines to supply a voltage

to the integrator. The integrator's output voltage will increase/decrease in response to the input voltage applied. Therefore, the control system can be programmed to track the low frequency variations and maintain the correct operating point.
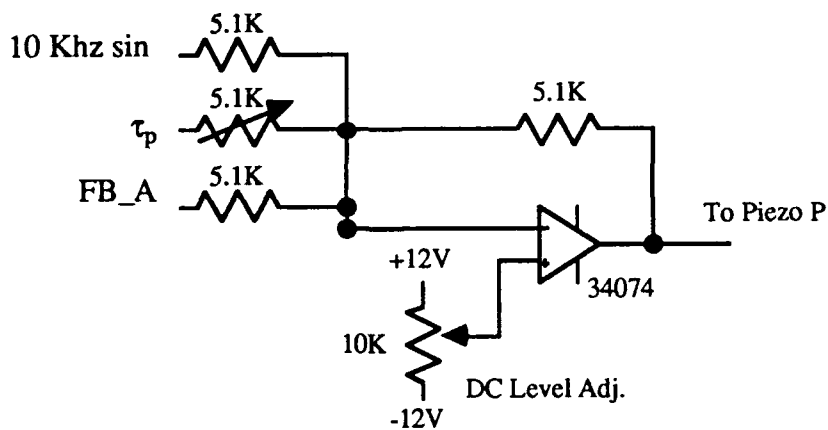
a.
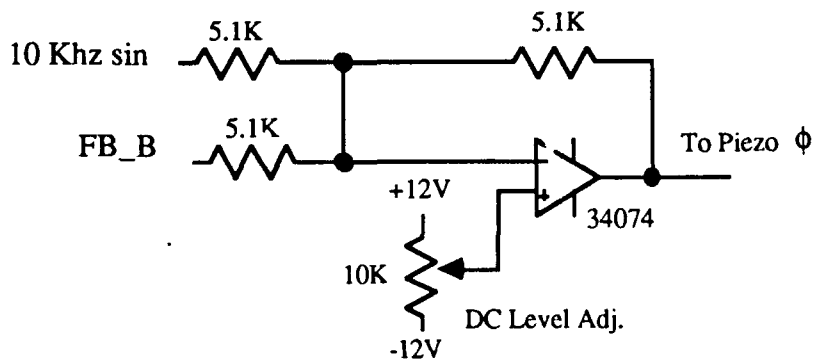
b.

Fig. B-7. The Summing Amplifiers. a.) The Sensing
Circuit Amp. b.) The Compensating Circuit
Amp.

Summing Amplifier--The summing amplifier is designed from a Motorola MC-34074AP Operational Amplifier. It combines and scales the control feedback, dither, and electro-optic feedback to maintain a bias control voltage on the ϕ- and P-phase modulators. The control voltage locks the sensor output at its maximum sensitive, common-mode compensated point.

Bibliography

[1] Buckman, A. B., "Analysis of a novel fiber interferometer with common-mode compensation," J. Lightwave Technology, Vol. LT-7, (1989), p. 151-7.

[2] Buckman, A. B., Pritchett, D. G., and Park, K., "Sensitivity-Enhanced, Common-mode Compensated Mach-Zehnder Fiberoptic Sensor Circuit with Electrooptic Feedback," Optic Letters, Vol. 14, No. 16, August 1989, p. 886-888.

[3] Giallorenzi, T. G., Bucaro, J. A., Dandridge, A., Sigel, G. H., Cole, J. H., Rashleigh, S. C., and Priest, R. G., "Optical Fiber Sensor Technology," IEEE J. Quantum Electronics, QE-18, April 1982, p. 626-65.

[4] De Paula, R. P. and Moore, E. L., "Fiber Optic Sensor Overview," SPIE Vol. 566, Fiber Optic and Laser Sensors III, (1985), p. 2-15.

[5] "Fiber optics found in sensor applications," American Ceramic Society Bulletin 68, September 1989, p. 1538.

[6] Krohn, D. A., "Fiber Optics Takes on Industrial Chore," Electron Products, Vol. 27, no. 13, December 12, 1984, p. 93-96.

[7] Mechanical Engineering Staff Report, "The Exciting Promise of Fiber Optic Sensors," Mechanical Engineering, Vol. 106, May 1984, p.60-5.

[8] Dakins, J. P., "Optical Fiber Sensors - Principles and Applications," Fibre Optics '83, SPIE, Vol. 374, April 1983, p. 19-21.

[9] Culshaw, B., Optical Fibre Sensing and Signal Processing, Peter Pereginus Ltd. (1984).

[10]   Jones, B. E. and Collier, S. J., "Optical Fiber Sensors Using Wavelength

Modulation and Simplified Spectral Analysis," J. Phys. E., Vol. 17, December

1984, p.1240-41.

[11]   Davis, C. M., Carome, E., Weik, M., Ezekiel, S., and Einzig, R., "Fiber-Optic

Sensor System Technology Assessment," Fiber-Optic Sensor Technology

Handbook, Dynamic Systems, Inc., McLean, VA 22101, (1982).

[12]   Dandridge, A. and Kersey, A. D., "Overview of Mach-Zehnder Sensor

Technology and Applications," Proc. Fiber Optic and Laser Sensors VI, SPIE

Vol. 985, Boston, September 1988, p. 34-52.

[13]   Jackson, D. A., Dandridge, A., and Sheem, S. K., "Measurement of Small

Phase Shifts Using A Single   Mode Optical Fiber Interferometer," Optic

Letters, Vol. 5, (1980), p. 139-41.

[14]   Stokes, L. F., Chadorow, M., and Shaw, H. J., "Sensitive All-Single-Mode

Fiber Resonant Ring Interferometer," J. Lightwave Technology, Vol. LT-1,

(1983), p. 110.

[15]   Jackson, D. A., Priest, R., Dandridge, A., and Tveten, A. B., "Elimination of

Drift in a Single-Mode Optical Fiber Interferometer Using a Piezoelectrically

Stretched Coiled Fiber," Applied Optics, Vol. 19, No. 17, September 1980,

p. 2926-2929.

[16]   Ibid., [2].

[17]   Ohtsuka, Y., "Analysis of a Fiber Optic Passive Loop Resonator Gyroscope:

Dependence on Resonator Parameters and Light Source Coherence," J.

Lightwave Technology, Vol. LT-3, (1985), p. 378.

[18]   Ibid., [15].

[19] Buckman, A. B., "General Sensitivity Enhancement and Common-Mode
Compensation Principle for Interferometric Fiber-Optic Sensors," IEEE J.
Lightwave Technology, Vol. LT-8, (1990), p. 1456-1460.

[20] Park, K., "Common-mode compensation in the 1.5 Mach Zehnder
Interferometer," Dissertation, University of Texas at Austin, 1989.

[21] Ibid., [15].

[22] Ibid., [15].

[23] Pritchett, D.G., "The Analysis of the Fiber optic 1.5 Mach Zehnder
Interferometric Sensor System," Dissertation, University of Texas
at Austin, 1989.

[24] Ibid., [14].

[25] Ibid., [15].

[26] Ibid., [10].

[27] Narayanan, C., "Analysis and Implementation of the Fiber Optic 1.5 Mach-
Zehnder Interferometric Intensity Sensor," Thesis, The University of Texas,
May 1990.

[28] Ibid., [15].

[29] Stowe, D. W., Moore, D. R., and Priest, R. G., "Polarization Fading in Fiber
Interferometric Sensors," IEEE J. Quantum Electornics, Vol. QE-18, No. 10,
October 1982, p. 1644-47.

[30] Ibid., [14].

[31] Sheem, S. K., Giallorenzi, T. G., and Koo, K. P., "Optical techniques to solve
the fading problem in fiber interferometers," Applied Optics, Vol. 21, (1982),
p. 689.

[32] Ibid., [15].

[33] Ibid., [15].

[34] Ibid., [15].

[35] Ibid., [15].

[36] Zhang, M. and Garmire, E., "Single-mode fiber-film directional coupler," IEEE J. Lightwave Technology, Vol. LT-5, (1987), p. 260.

[37] Ibid., [15].

[38] Dagenais, D. M., Bucholtz, F., Koo, K. P., and Dandridge, A., " " Electron. Lett., Vol. 24, 1988, p. 1422-23.

[39] Koo, K. P., Bucholtz, F., and Dandridge, A., Optics Letters, Vol. 11, 1986, p. 683-685.

[40] Brown, D. A., Hofler, T., and Garrett, S. L., Fiber and Integrated Optics, Vol. 8, 1989, p. 168-91.

[41] Ibid., [15].

[42] Ibid., [38-40].

Vita

Booker Howell Tyrone, Jr. was born in San Antonio, Texas on December 4, 1952 to Booker, Sr. and Hattie Marie Tyrone. After graduating from Sam Houston High School, San Antonio, Texas in 1971, he enlisted in the U.S. Air Force. He completed technical training in radar maintenance at Keesler AFB, Mississippi and worked as a radar technician at Fort Meade, Maryland and Hofn, Iceland. Returning to Keesler AFB, Mississippi in 1977, he worked as a technical instructor in radar until August 1978 when he entered the University of Texas at Austin (UT) under U.S. Air Force sponsorship. He graduated from UT with a Bachelor of Science degree in Electrical Engineering in December 1980. After completion of Officer Training School at Lackland AFB, Texas, he was commissioned as a second lieutenant in the U.S. Air Force and assigned to Holloman AFB, New Mexico. He worked as an Inertial Guidance Analyst from June 1981 until he became a Guidance Program Test Director in 1983. In January 1985 he entered Graduate School at the University of Texas at Austin where he majored in Communications and Controls with a minor in Mathematics. He graduated in August 1986 with a Master of Science degree in Electrical Engineering and joined the faculty of the U.S. Air Force Academy (USAFA), Colorado Springs, Colorado as an instructor in the Electrical Engineering department. He taught for two years and returned to UT in June 1988 to continue studying toward the degree of Doctor of Philosophy in Electrical Engineering.

Permanent address: 639 Lincolnshire Drive
                   San Antonio, TX 78220

This dissertation was typed by the author.